ARTICLES
https://doi.org/10.1038/s41593-018-0283-1
nature neuroscience

Locus coeruleus activation enhances thalamic feature selectivity via norepinephrine regulation of intrathalamic circuit dynamics

Charles Rodenkirch, Yang Liu, Brian J. Schriver and Qi Wang *

We investigated locus coeruleus (LC) modulation of thalamic feature selectivity through reverse correlation analysis of single-unit recordings from different stages of the rat vibrissa pathway. LC activation increased feature selectivity, drastically improving thalamic information transmission. We found that this improvement was dependent on both local activation of α-adrenergic receptors and modulation of T-type calcium channels in the thalamus and was not due to LC modulation of trigeminothalamic feedforward or corticothalamic feedback inputs. Tonic spikes with LC stimulation carried three times the information as did tonic spikes without LC stimulation. Modeling confirmed norepinephrine regulation of intrathalamic circuit dynamics led to the improved information transmission. Behavioral data demonstrated that LC activation increased the perceptual performance of animals performing tactile discrimination tasks through LC–norepinephrine optimization of thalamic sensory processing. These results suggest a new subdimension within the tonic mode in which brain state can optimize thalamic sensory processing through modulation of intrathalamic circuit dynamics.

Neuromodulatory systems, such as the locus coeruleus (LC)–norepinephrine (NE) system, are integral in the modulation of behavioral state, which in turn exerts a heavy influence on sensory processing, perception, and behavior[1–8]. For example, arousal, alertness, and locomotion are typically correlated with significantly elevated sensory evoked neural responses[3–5]. The LC is the primary source of NE to the forebrain[9,10]. LC neurons exhibit constant tonic firing at low frequencies, with frequency correlating with arousal level, behavioral performance[11], and NE concentration in the brain[12]. NE has been shown to alter neuronal excitability[13], suggesting that the LC–NE system produces state-dependent modulatory effects on sensory processing and thus perception. The precise mechanism underlying LC–NE modulation of stimulus feature representation in the various stages of sensory processing that underlies perception, however, remains elusive.

It is well established that the thalamus plays an essential role in gating the flow of sensorimotor information to the neocortex, serving to establish cortical representation of the sensorimotor environment[14–17]. Thalamocortical information transmission has been proposed to be strongly modulated by the dynamic interplay between the thalamic relay nucleus and the GABAergic thalamic reticular nucleus (TRN)[18,19]. Neurons in the early stages of sensory pathways selectively respond to specific features of sensory stimuli[20–22]. In the rodent vibrissa pathway, thalamocortical neurons in the ventral posteromedial nucleus (VPm) encode kinetic features of whisker movement[20], allowing stimuli to be represented by distinctive, temporally precise firing patterns. Therefore, understanding feature selectivity is crucial to understanding sensory processing and perception.

Here we examine the mechanism underlying LC modulation of thalamic feature selectivity and tactile perception through reverse correlation analysis of single-unit recordings taken from different stages of the rat vibrissa pathway while LC activation conditions were systematically varied. Our results demonstrated an LC-activation-induced decrease in firing rate, coupled with an increase in the feature selectivity of VPm neurons, resulting in a dramatic increase in both information transmission efficiency and rate. Surprisingly, recordings in the projecting principal trigeminal nucleus (PrV) revealed LC activity did not modulate PrV sensory information transmission, suggesting the observed increase in thalamic feature selectivity was not trivially inherited from the PrV. Inactivation of the cortical column, topographically aligned with the VPm neuron being recorded, did not affect LC-activation-induced improvement of thalamic feature selectivity, indicating that corticothalamic feedback did not play a role in this improvement.

LC activation reduced burst firing for both VPm and TRN neurons. However, VPm tonic spikes without LC stimulation carried only ~30% of the information of those during 5 Hz LC stimulation, suggesting LC-activation-improved information transmission was not a result of simply switching thalamic firing to tonic mode. Blocking thalamic T-type calcium channels suppressed burst firing and eliminated LC-activation-induced improvement of thalamic information transmission, indicating that this LC-linked improvement results from suppression of T-channel activity by NE regulation of thalamoreticulo–thalamic circuit dynamics. Modeling results showed that NE effects in solely the VPm or TRN could not account for the dramatic increase in information transmission, suggesting that concurrent LC–NE modulation of both the VPm and TRN is necessary to alter intrathalamic circuit dynamics for optimal thalamic information transmission. Furthermore, we found that LC activation also increased perceptual sensitivity for animals performing a tactile discrimination task. This behavioral improvement was blocked when NE effects in the thalamus were pharmacologically precluded, confirming that LC–NE modulation of the thalamic sensory processing is critical to the LC-activation-induced improvement in perception. These findings reveal a novel mechanism through which LC activation enhances thalamic sensory processing and perceptual performance, and suggest a brain-state-dependent subdimension in the tonic mode of thalamic firing.

Department of Biomedical Engineering, Columbia University, New York, NY, USA. *e-mail: qi.wang@columbia.edu

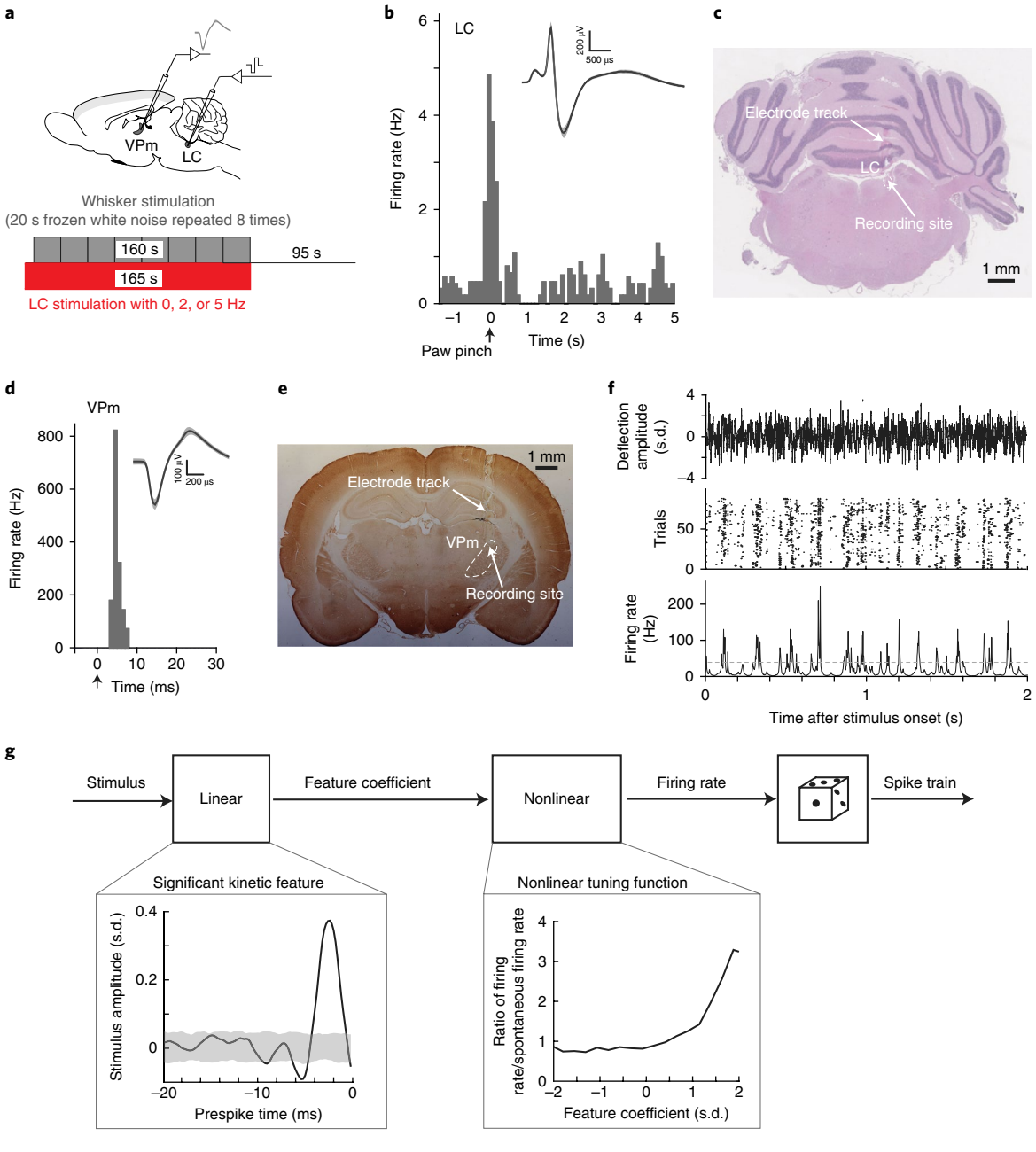

Fig. 1 | White noise reverse-correlation analysis for estimation of thalamic feature selectivity during different LC activation conditions. a, Schematic of experimental setup and stimulation framework (adapted from a rat brain atlas). **b**, Example of phasic LC firing followed by inhibition in response to paw pinch. Inset: example wide LC waveform; shaded area represents ±s.d. ($n = 70$ spikes). **c**, Histological confirmation of correct electrode placement in the LC. **d**, Example single-unit VPm response to a punctate stimulation of its principal whisker, with arrow marking stimulation onset. Inset: example VPm waveform; shaded area represents ±s.d. ($n = 48$ spikes). **e**, Histological confirmation of correct electrode placement in the VPm. **f**, Top: clip from one of the frozen WGN stimuli used for reverse-correlation analysis. Middle: example raster plot of the response of a VPm neuron to the whisker stimulation shown above. Bottom: SDF created from the response of the same VPm neuron. Dashed line indicates the threshold used to define events. **g**, Diagram of the linear–nonlinear–Poisson cascade model used to characterize thalamic feature selectivity. Boxes: example kinetic feature and corresponding nonlinear tuning function for a VPm neuron recovered using white Gaussian noise reverse-correlation analysis. Shaded area indicates 99.9% confidence interval.

Results

We microstimulated the LC of pentobarbital-anesthetized rats while recording single-unit activity from the VPm in the rat vibrissa pathway (Fig. 1a). Placement of the stimulating electrode into the LC was verified via electrophysiology and histology (Fig. 1b,c and Methods). All LC neurons used to initially confirm electrode location in the LC exhibited the usual hallmarks: a phasic response to paw pinch followed by a period of inhibition, and a wide spike waveform[23] (Fig. 1b). VPm neurons were identified by their depth, waveform, and reliable, short-latency response to a brief deflection of their principal whisker[17] (Fig. 1d). On a subset of experiments, correct placement of the stimulating and recording electrodes was further confirmed by post-mortem histological analysis (Fig. 1c,e).

LC activation improved VPm feature selectivity while decreasing firing rate. To study how the LC–NE system modulates the coding properties of thalamic relay neurons and the information

they transmit, single-unit extracellular recordings of VPm neurons, lasting ~2 h, were acquired (Supplementary Fig. 1a). During these recordings, we randomly cycled through 3 varying conditions of LC activation: 0 (that is, no LC stimulation, as a control), 2, and 5 Hz and mechanically stimulated the principal whisker with low-pass filtered frozen white Gaussian noise (WGN) (Fig. 1a, Supplementary Fig. 1b, and Methods). Each LC activation condition was repeated multiple times throughout each recording (range of 3–13 repetitions, average of 5.6 ± 0.6 repetitions; mean ± s.e.m. reported for all results unless otherwise stated). During control conditions, VPm neurons were highly responsive to WGN whisker stimulation, firing in a reliable, temporally precise fashion at certain events in the stimulus[24] (Fig. 1f). White noise reverse correlation analysis allowed us to recover the kinetic features of the whisker movement to which VPm neurons were significantly sensitive to (Fig. 1g and Methods). A VPm neuron's feature selectivity can be represented by a set of kinetic features it is sensitive to, coupled with a corresponding set of nonlinear tuning functions that map the neuron's firing rate response versus how similar the stimulus is to that feature (that is, the first and second components of Fig. 1g, respectively).

When we examined the effects of LC activation on thalamic response to stimuli, we found that LC activation significantly reduced the firing rate of VPm neurons in response to WGN whisker stimulation (Fig. 2a). LC activation did not induce changes in the shape of the kinetic features for which a neuron was selective; however, we did find that the amplitude of the recovered features increased in an LC-activation-frequency-dependent manner (Fig. 2b). To quantify this modulation of the recovered features, we computed the feature modulation factor, defined as the dot product of a feature recovered under control conditions with that from LC activation conditions normalized by the dot product of the control condition recovered feature with itself (see Methods). A feature modulation factor of 1 would indicate that LC activation had no effect on the recovered features. If the amplitude of the recovered feature increased, then the feature modulation factor would also increase. Indeed, we found that 2- and 5-Hz LC activation resulted in significantly increased feature modulation factors of approximately 15% and 47%, respectively (Fig. 2c). We also calculated the average peak-to-peak amplitude of the features that the VPm encoded. Consistent with the feature modulation factor, the average peak-to-peak amplitude also increased with the frequency of LC activation (Supplementary Fig. 2a).

Having determined the encoded feature set for each VPm neuron under each LC activation condition, we were then able to calculate the corresponding nonlinear tuning functions[20]. Interestingly, we found that LC activation resulted in a change in the nonlinear tuning functions of VPm neurons that indicated an increased selectivity of response to the specific features encoded by the VPm neurons (Fig. 2d).

To quantify the effects of the LC activation on thalamic transmission of information about the absence/presence of the encoded kinetic feature(s), we used an information theoretic approach[20,25]. We found that 2 and 5 Hz LC stimulation drastically increased the information that each spike conveyed (Fig. 2e and Supplementary Fig. 2b). Interestingly, despite the reduction in VPm firing rate, LC activation also resulted in a more than twofold increase in information transmission rate (bits s^{-1}) (Supplementary Fig. 2c).

To rule out the possibility that the observed phenomenon was due to inadvertent stimulation of brainstem nuclei adjacent to the LC, optogenetic LC stimulation was used on a subset of experiments. We selectively expressed channelrhodopsin 2 (ChR2) in LC neurons by injecting a lentivirus with a PRSx8 promoter that is selective for LC–NE neurons (pLenti-PRSx8-hChR2(H134R)-mCherry) into the LC[26]. On a subset of animals, we validated the selectivity with post-mortem immunohistological analysis (Fig. 2f,g). Four weeks after transfection, we performed the same white noise reverse correlation experiment while varying LC-activation conditions, as detailed above, except photostimulation was used to activate the LC instead of electrical microstimulation. These experiments showed a LC-photoactivation-dependent decrease in firing rate (Fig. 2h), increase in feature selectivity (Supplementary Fig. 3a), increase in feature modulation factor (Fig. 2i), increase in information transmission (Fig. 2j and Supplementary Fig. 3b), and increase in information transmission rate (Supplementary Fig. 3c). This confirmed the effects of electrical microstimulation of the LC on thalamic information transmission were due to selective LC activation and unlikely due to the inadvertent activation of the adjacent nuclei or axons of passage.

To rule out the possibility that the observed phenomenon was an artifact of anesthesia and to ensure the observed phenomenon generalizes to awake animals, we recorded the response of VPm neurons to repeated WGN stimulation of their principal whisker in awake, head-fixed rats (Supplementary Fig. 4a and Methods) while modulating LC activity either electrically or optogenetically. In awake rats, we found that LC activation still induced an increase in feature selectivity (Supplementary Fig. 4b) as well as an increase in the feature modulation factor (Supplementary Fig. 4c). Further we observed a similar LC-activation-induced increase in information transmission (Supplementary Fig. 4d), confirming that LC activation enhancing thalamic information transmission is a general phenomenon.

Improved thalamic feature selectivity and information transmission by LC activation was not inherited from the projecting trigeminal input. Although LC activation resulted in a strong modulation of VPm neurons' coding properties, it was not clear whether the mechanism underlying this modulation was occurring directly in the thalamus, or at previous stages of the pathway. To investigate this possibility, we recorded single-unit activity in the PrV of the vibrissa system, which projects and provides direct feedforward excitatory input to the VPm in the vibrissa pathway (Fig. 3a and Supplementary Fig. 5a).

Interestingly, we found that LC activation did not have any significant effect on the feature selectivity of PrV neurons (Fig. 3b). Further, we observed no LC-activation-induced difference in PrV firing rate (Supplementary Fig. 5b) or change in feature modulation factor (Fig. 3c). Consequently, there was no LC-activation-induced increase in information transmission efficiency (Fig. 3d and Supplementary Fig. 5c).

LC-activation-induced improvement of thalamic feature selectivity and information transmission was not due to corticothalamic feedback. Previous studies have found that the deep cortical layers send dense projections to the thalamus[27]. As the LC also innervates the cortex, it could be possible that LC activation alters corticothalamic feedback in a way that results in an increase in the information transmitted by thalamocortical neurons. To test the extent to which corticothalamic feedback plays a role in the LC-activation-induced increase in VPm feature selectivity, we silenced the cortex in a subset of rats to remove its possible influence on LC-activation-induced changes in thalamic processing. We initially mapped the barrel columns (Supplementary Fig. 6a), then injected muscimol into the center of the cortical craniotomy. In two animals, we confirmed that intracortical muscimol silenced the cortex, as we observed no evoked spiking activity or local field potential (LFP) response in the central column or adjacent columns (Supplementary Fig. 6b). We then performed single-unit recording in the VPm barreloid topographically aligned with the barrel column in which the injection was made.

Interestingly, we found that cortical inactivation also had no effects on the LC-activation-induced increase in thalamic feature selectivity and information transmission. We still observed the same LC-activation-induced increase in feature sensitivity following

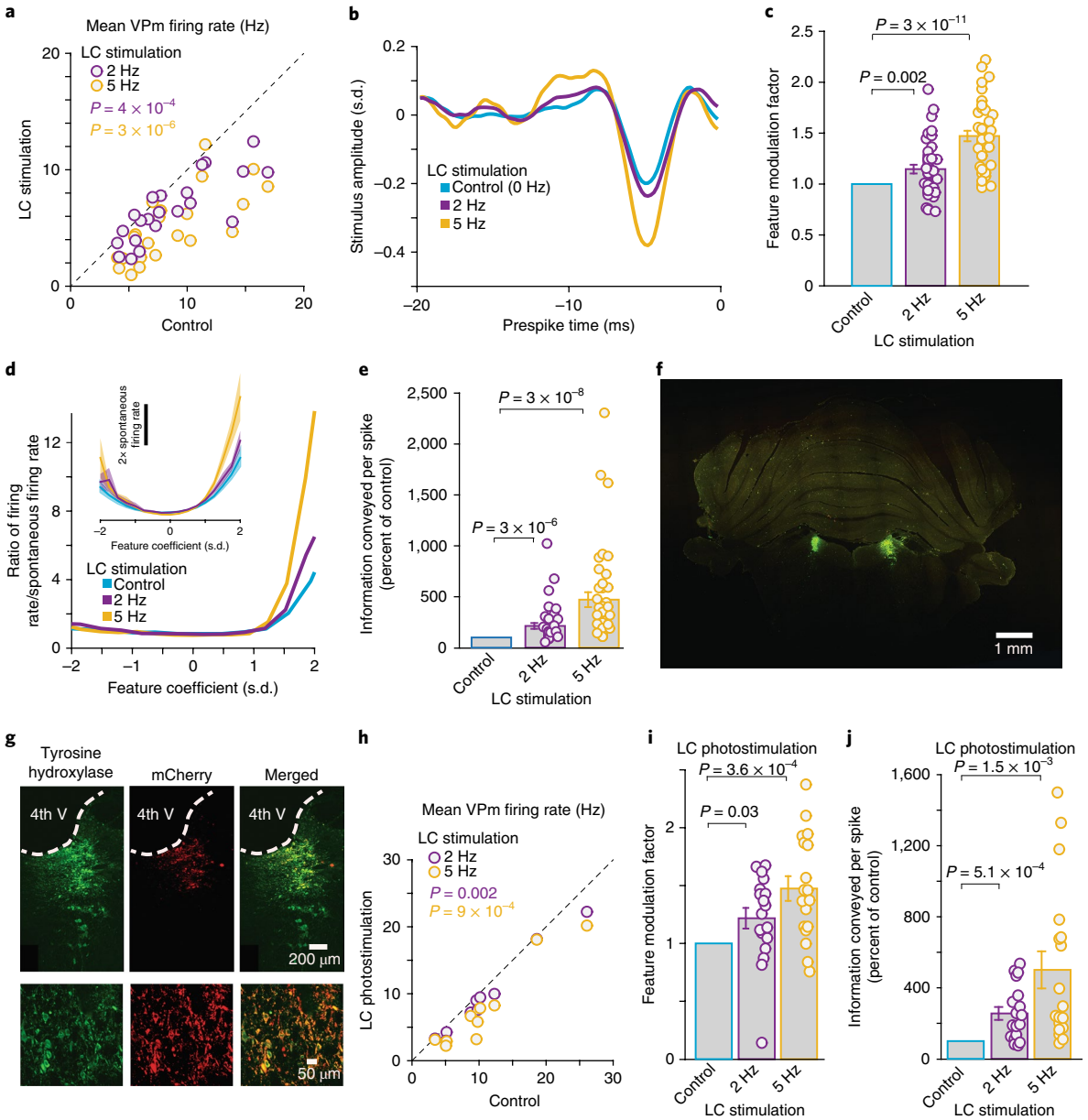

Fig. 2 | LC activation increased VPm feature selectivity and improved information transmission while decreasing firing rate. a, Summary of VPm firing rate in response to WGN whisker stimulation under varying LC stimulation conditions. Each circle represents a VPm neuron (8.5 ± 0.8 Hz without LC stimulation vs. 6.4 ± 0.6 Hz during 2-Hz LC stimulation and 5.0 ± 0.6 Hz during 5-Hz LC stimulation, $n = 22$ neurons across 15 animals, Bonferroni corrected $\alpha = 0.025$, $P = 3.1 \times 10^{-4}$ and 2.5×10^{-6}, respectively, paired t test). **b**, Example of recovered features of a VPm neuron under varying LC stimulation conditions. **c**, Population average of feature-modulation factor for VPm neurons under varying LC stimulation conditions. Each circle represents a significant feature (1 without LC stimulation vs. 1.15 ± 0.04 during 2-Hz LC stimulation and vs. 1.47 ± 0.05 during 5-Hz LC stimulation, $n = 41$ features across 22 neurons across 15 animals, Bonferroni corrected $\alpha = 0.025$, $P = 1.5 \times 10^{-3}$ and 2.3×10^{-11}, respectively, paired t test). **d**, Example of nonlinear tuning functions, corresponding to the features shown in Fig. 2b. Inset: the population average nonlinear tuning functions under varying LC stimulation conditions. **e**, Normalized changes in information transmission efficiency (bits per spike) for VPm neurons under varying LC stimulation conditions. Each circle represents a significant feature (213 ± 29% of the control during 2-Hz LC stimulation and 469 ± 72% of the control during 5-Hz LC stimulation, $n = 41$ features across 22 neurons across 15 animals, Bonferroni corrected $\alpha = 0.025$, $P = 2.9 \times 10^{-6}$ and 2.5×10^{-8}, respectively, Wilcoxon signed-rank test). **f**, LC locations were confirmed by tyrosine hydroxylase immunoreactivity (green) in a coronal section. **g**, Histological confirmation of selective transgene expressions in LC neurons. Left: tyrosine hydroxylase labels LC neurons. Middle: viral mCherry reporter expression. Right: merged image shows colocalization. Similar results were observed in two other animals. 4th V, fourth ventricle. **h**, Summary of VPm firing rate in response to WGN whisker stimulation under varying LC photostimulation conditions. Each circle represents a VPm neuron (10.9 ± 2.2 Hz without LC stimulation vs. 9.4 ± 2.0 Hz during 2-Hz LC stimulation and 7.8 ± 2.0 Hz during 5-Hz LC stimulation, $n = 10$ neurons across 4 animals, Bonferroni corrected $\alpha = 0.025$, $P = 2.1 \times 10^{-3}$ and 9.0×10^{-4}, respectively, paired t test). **i**, Population average of feature modulation factor for VPm neurons under varying LC photostimulation conditions. Each circle represents a significant feature (1 without LC stimulation vs. 1.22 ± 0.09 during 2-Hz LC stimulation and 1.47 ± 0.11 during 5-Hz LC stimulation, $n = 18$ features across 10 neurons across 4 animals, Bonferroni corrected $\alpha = 0.025$, $P = 0.026$ and 3.6×10^{-4}, respectively, paired t test). **j**, Normalized changes in information transmission efficiency (bits per spike) for VPm neurons under varying LC photostimulation conditions. Each circle represents a significant feature (256 ± 36% of the control during 2-Hz LC stimulation and 501 ± 104% of the control during 5-Hz LC stimulation, $n = 18$ features across 10 neurons across 4 animals, Bonferroni corrected $\alpha = 0.025$, $P = 5.1 \times 10^{-4}$ and 1.4×10^{-3}, respectively, paired t test). Error bars and shaded area indicate ±s.e.m.

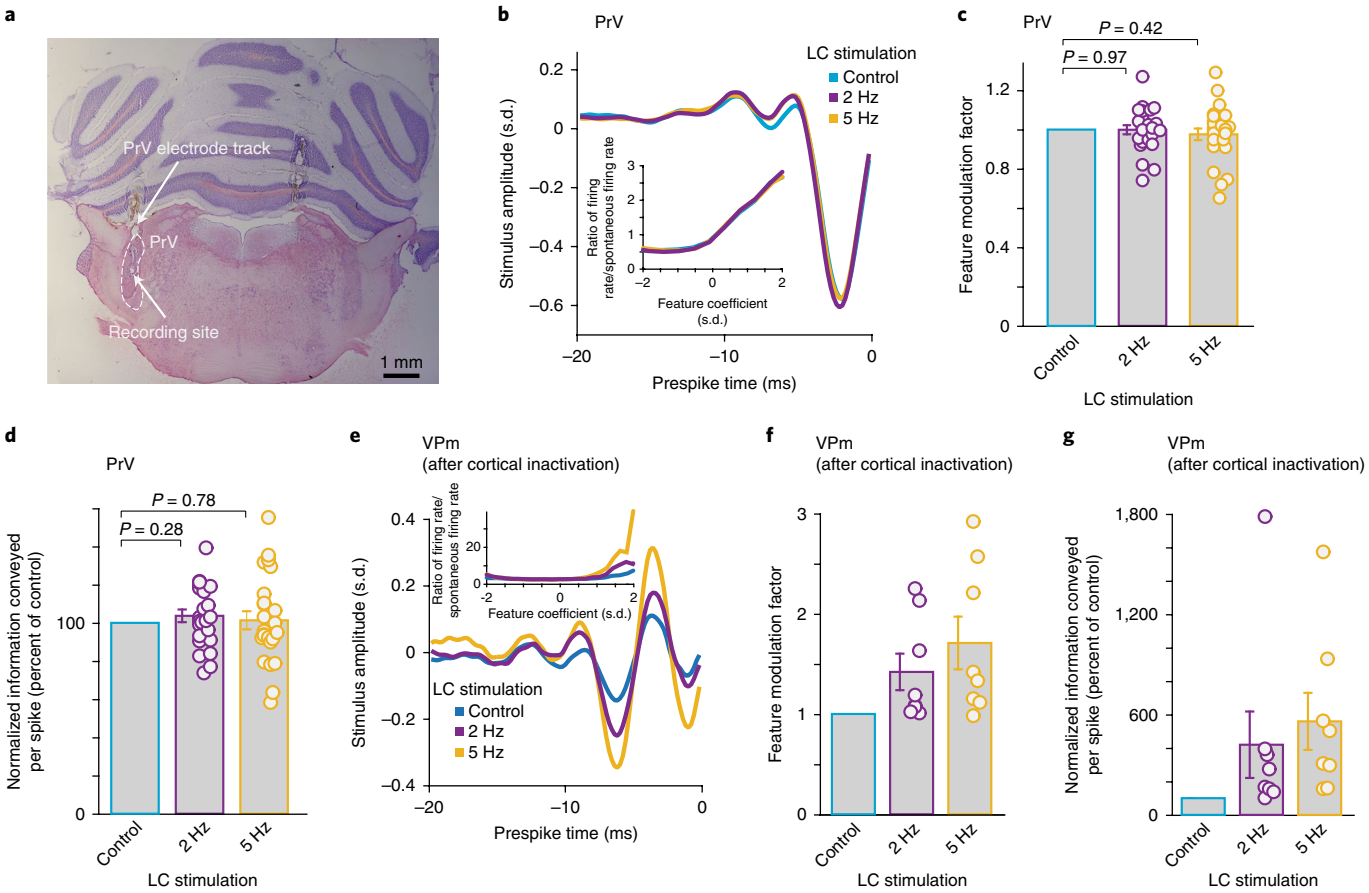

Fig. 3 | LC-activation-induced increase in thalamic information transmission was not due to modulation of the trigeminothalamic feedforward or corticothalamic feedback inputs. a, Histological confirmation of correct electrode placement in the PrV. **b**, Example of recovered features for a PrV neuron under varying LC stimulation conditions. Inset: corresponding nonlinear tuning functions. **c**, Population average of feature-modulation factor for PrV neurons under varying LC stimulation conditions. Each circle represents a significant feature (1 without LC stimulation vs. 1.0 ± 0.02 during 2-Hz LC stimulation and vs. 0.98 ± 0.03 during 5-Hz LC stimulation, $n = 24$ features across 13 neurons across 8 animals, Bonferroni corrected $\alpha = 0.025$, $P = 0.97$ and 0.42, respectively, paired t test). **d**, Normalized change in information transmission efficiency (bits per spike) for PrV neurons under varying LC stimulation conditions. Each circle represents a significant feature (104 ± 3% of the control during 2-Hz LC stimulation and 101 ± 5% of the control during 5-Hz LC stimulation, $n = 24$ features across 13 neurons across 8 animals, Bonferroni corrected $\alpha = 0.025$, $P = 0.28$ and 0.78, respectively, paired t test). **e**, Example of recovered features for a VPm neuron, post-cortical inactivation, under varying LC stimulation conditions. Inset: corresponding nonlinear tuning functions. **f**, Population average of feature modulation factor for VPm neurons, post-cortical inactivation, under varying LC stimulation conditions. Each circle represents a significant feature (1 without LC stimulation vs. 1.42 ± 0.18 during 2-Hz LC stimulation and vs. 1.71 ± 0.26 during 5-Hz LC stimulation, $n = 8$ features across 7 neurons across 4 animals, Bonferroni corrected $\alpha = 0.025$, $P = 0.055$ and 0.031, respectively, paired t test). **g**, Population average of information transmission efficiency (bits per spike) for VPm neurons, post-cortical inactivation, under varying LC stimulation conditions. Each circle represents a significant feature (430 ± 199% of the control during 2-Hz LC stimulation and 560 ± 171% of the control during 5-Hz LC stimulation, $n = 8$ features across 7 neurons across 4 animals, Bonferroni corrected $\alpha = 0.025$, $P = 0.15$ and 0.031, respectively, paired t test). Error bars indicate ±s.e.m.

muscimol injection to the cortex (Fig. 3e) as well as an LC-activation-induced increase in feature modulation factors (Fig. 3f) and increase in information transmission (Fig. 3g and Supplementary Fig. 6c).

LC-activation-induced improvement of thalamic information transmission resulted from the action of NE on α-adrenergic receptors in the thalamus. As the LC projects to other neuromodulatory systems[28], it is unclear whether direct (NE action in the thalamus) or indirect (action of other neuromodulators indirectly released by LC activation) effects of LC activation, or a combination of both, was responsible for the improved thalamic information transmission. To test the extent to which noradrenergic receptor activation was involved in enhancing thalamic information transmission by LC activation, we blocked α-adrenergic receptors in the thalamus by injecting phentolamine[29]. LC electrode position was further confirmed by a VPm recording before phentolamine injection that showed an LC-activation-dependent increase in feature selectivity (Fig. 4a). Before phentolamine injection, the same trend of increase was present for feature modulation factors (Fig. 4b) and information transmission (Fig. 4d and Supplementary Fig. 7a).

We then slowly injected the α-adrenergic receptor antagonist phentolamine (2 µl, 100 nl min^{-1}, 10 mM) into the thalamus. Following phentolamine injection into the thalamus, LC activation no longer had any effect on feature selectivity (Fig. 4c), indicating that α-adrenergic receptor activation is primarily responsible for the observed effects of LC activation on thalamic processing. With phentolamine, we saw no LC-stimulation-induced change in the feature modulation factor (Fig. 4b), and no change in information transmission (Fig. 4d and Supplementary Fig. 7b). Moreover, we tested the effects of LC activation following saline injection and found the same LC-activation-induced improvement of information transmission in the VPm, confirming that the disappearance of

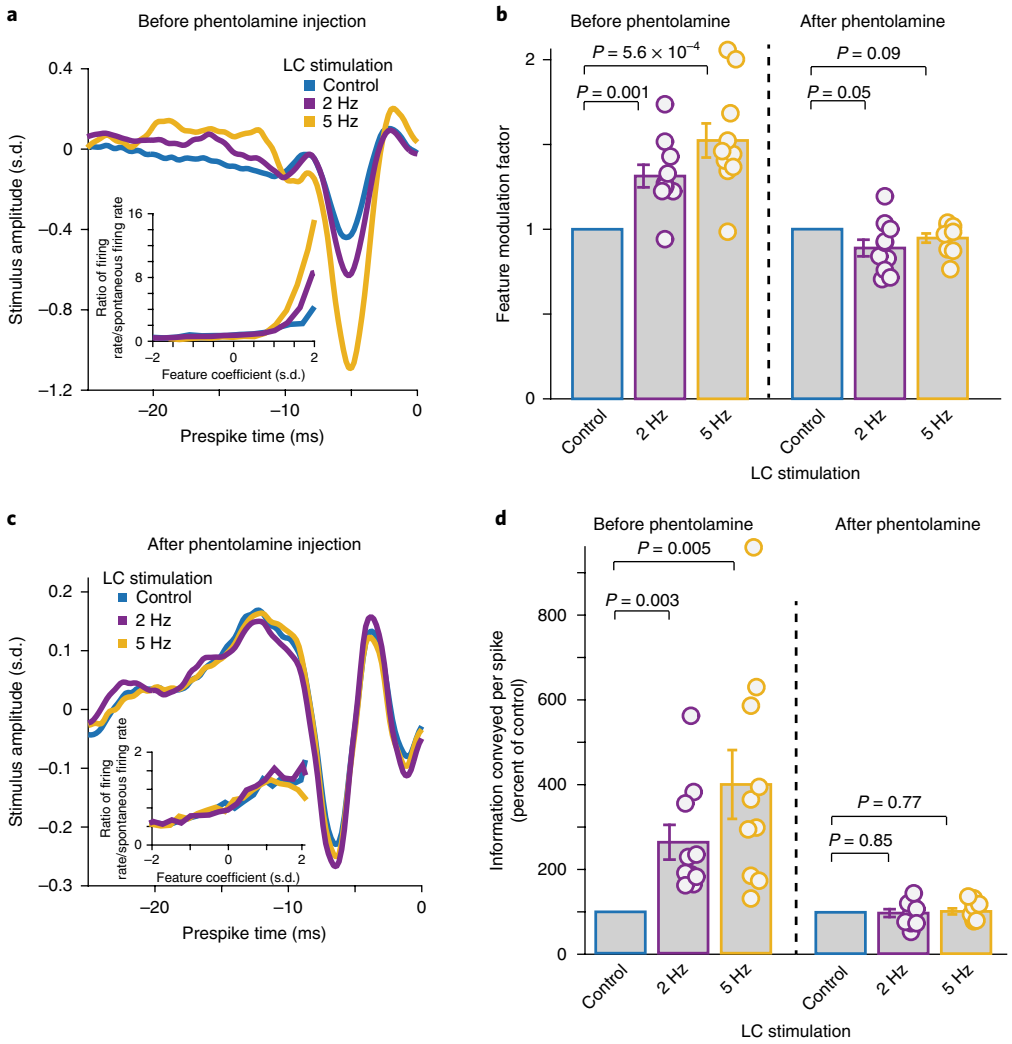

Fig. 4 | LC-activation-induced increase in thalamic information transmission was dependent on the action of alpha-adrenergic receptors in the thalamus. a, Example of recovered features for a VPm neuron, before phentolamine injection, under varying LC stimulation conditions. Inset: corresponding example nonlinear tuning functions. **b**, Population average of feature-modulation factor under varying LC stimulation conditions. Each circle represents a significant feature. Left: VPm neurons, before phentolamine injection (1 without LC stimulation vs. 1.31 ± 0.07 during 2-Hz LC stimulation and vs. 1.52 ± 0.10 during 5-Hz LC stimulation, $n = 10$ features across 6 neurons across 4 animals, Bonferroni corrected $\alpha = 0.025$, $P = 1.1 \times 10^{-3}$ and $P = 5.6 \times 10^{-4}$, respectively, paired t test). Right: VPm neurons, after phentolamine injection (1 without LC stimulation vs. 0.89 ± 0.05 during 2-Hz LC stimulation and vs. 0.95 ± 0.03 during 5-Hz LC stimulation, $n = 10$ features across 5 neurons across 4 animals, Bonferroni corrected $\alpha = 0.025$, $P = 0.05$ and $P = 0.09$, respectively, paired t-test). **c**, Example of recovered features for a VPm neuron, after phentolamine injection, under varying LC stimulation conditions. Inset: corresponding nonlinear tuning functions. **d**, Population average of information transmission efficiency (bits per spike) under varying LC stimulation conditions. Left: VPm neurons, before phentolamine injection ($264 \pm 41\%$ of the control during 2-Hz LC stimulation and $401 \pm 81\%$ of the control during 5-Hz LC stimulation, $n = 10$ features across 6 neurons across 4 animals, Bonferroni corrected $\alpha = 0.025$, $P = 3.1 \times 10^{-3}$ and $P = 5.0 \times 10^{-3}$, respectively, paired t test). Right: VPm neurons, after phentolamine injection. Each circle represents a significant feature ($98 \pm 9\%$ of the control during 2-Hz LC stimulation and $102 \pm 7\%$ of the control during 5-Hz LC stimulation, $n = 10$ features across 5 neurons across 4 animals, Bonferroni corrected $\alpha = 0.025$, $P = 0.85$ and $P = 0.77$ respectively, paired t test). Error bars indicate ±s.e.m.

LC effects on thalamic information processing with phentolamine injection was not due to possible damage inflicted by the injection (Supplementary Fig. 7c).

Increased information transmission did not result from gain reduction or changes in signal-to-noise ratio. When investigating how the LC-activation-induced change in VPm response led to increased feature selectivity and information transmission, we first asked whether suppression of VPm firing rate could provide an explanation. To test this, a computational control was conducted in which we randomly deleted spikes from the control VPm spike raster until the average firing rate of each spike raster was equalized to their corresponding 5 Hz LC stimulation spike raster's firing rate. We then computed the information that the firing-rate-matched spike train transmitted and found that simulated suppression of firing rate did not result in any significant increase in information transmission (Fig. 5a), ruling out gain reduction as a mechanism.

All VPm neurons produced a reliable response to specific kinetic features occurring at specific temporal locations in the WGN stimulus, resulting in many temporal response events present in the generated spike density functions (SDF). These events, defined by thresholding the SDF of the neurons response (Fig. 1f and see

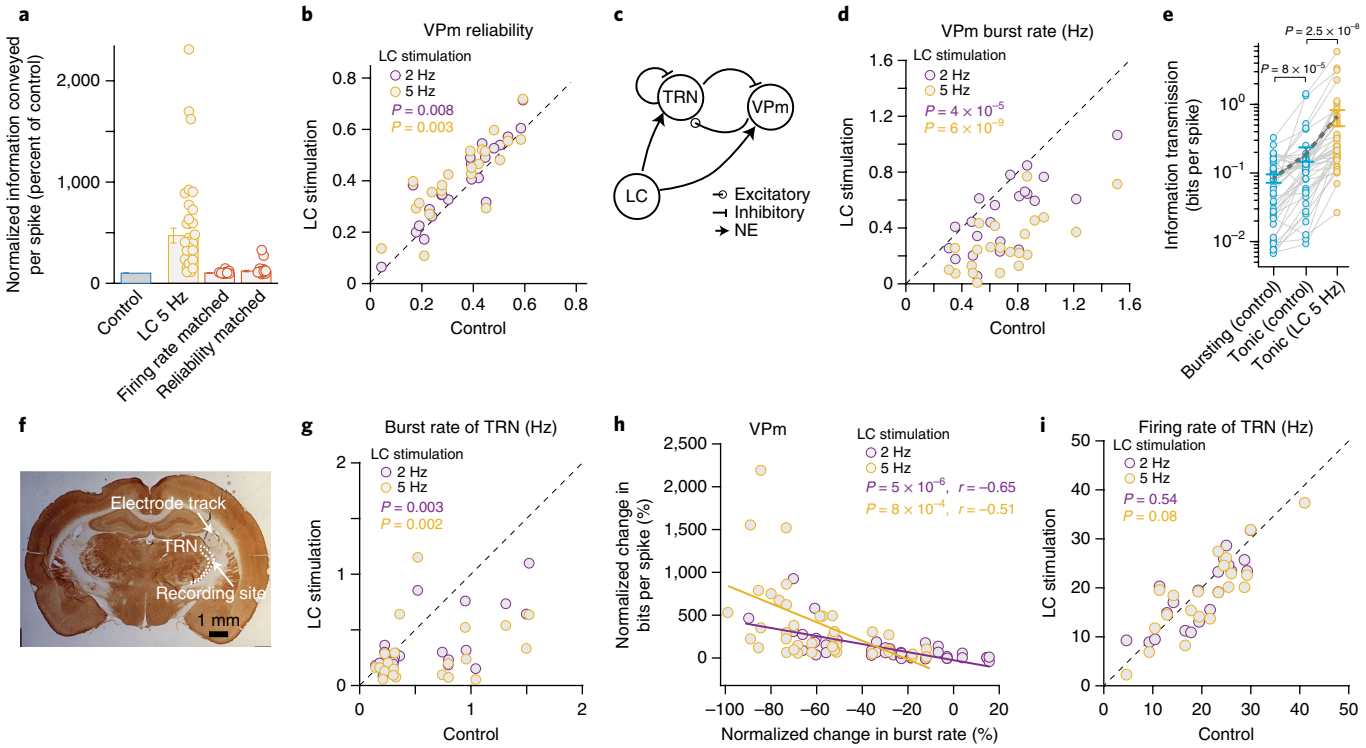

Fig. 5 | LC-activation modulated intrathalamic circuit dynamics. a, Population average of information transmission efficiency (bits per spike) for VPm neurons under varying LC stimulation conditions compared with simulated reductions in firing rate (102 ± 1% of the control, $n = 41$ features across 22 neurons across 15 animals, $\alpha = 0.05$, $P = 0.55$, Wilcoxon signed-rank test) and increases in reliability (121 ± 7% of the control, $n = 41$ features across 22 neurons across 15 animals, $\alpha = 0.05$, $P = 3.7 \times 10^{-6}$, Wilcoxon signed-rank test). **b**, LC activation significantly improved the reliability of the VPm response to WGN whisker stimulation. Each circle represents a VPm neuron (0.35 ± 0.03 without LC stimulation vs. 0.39 ± 0.03 during 2-Hz LC stimulation and vs. 0.41 ± 0.03 during 5-Hz LC stimulation, $n = 22$ neurons across 15 animals, Bonferroni corrected $\alpha = 0.025$, $P = 8.0 \times 10^{-3}$ and $P = 2.6 \times 10^{-3}$, respectively, paired t test). **c**, Diagram of the reciprocal connection between the VPm and TRN, both of which are recipient of LC projections. **d**, Summary of VPm burst rate in response to WGN whisker stimulation under varying LC stimulation conditions. Each circle represents a VPm neuron (0.71 ± 0.06 Hz without LC stimulation vs. 0.48 ± 0.05 Hz during 2-Hz LC stimulation and vs. 0.28 ± 0.04 Hz during 5-Hz LC stimulation, $n = 22$ neurons across 15 animals, Bonferroni corrected $\alpha = 0.025$, $P = 4.3 \times 10^{-5}$ and $P = 6.0 \times 10^{-9}$ respectively, paired t test). **e**, Comparison of information carried by bursting and tonic spikes without LC stimulation (0.08 ± 0.01 bits per spike vs. 0.19 ± 0.05 bits per spike, $n = 41$ features across 22 neurons across 15 animals, Bonferroni corrected $\alpha = 0.025$, $P = 8.0 \times 10^{-5}$, Wilcoxon signed-rank test) as well as information carried by tonic spikes with and without LC stimulation (0.19 ± 0.05 bits per spike without LC stimulation vs. 0.65 ± 0.17 bits per spike with 5-Hz LC stimulation, $n = 41$ features across 22 neurons across 15 animals, $\alpha = 0.05$, $P = 2.5 \times 10^{-8}$, Wilcoxon signed-rank test). **f**, Histological confirmation of correct electrode placement in the TRN. **g**, Summary of TRN burst rate in response to WGN whisker stimulation under varying LC stimulation conditions. Each circle represents a TRN neuron (0.62 ± 0.10 Hz without LC stimulation vs. 0.37 ± 0.06 Hz during 2-Hz LC stimulation and vs. 0.29 ± 0.06 Hz during 5-Hz LC stimulation, $n = 22$ neurons across 10 animals, Bonferroni corrected $\alpha = 0.025$, $P = 2.6 \times 10^{-3}$ and $P = 2.2 \times 10^{-3}$, respectively, paired t test). **h**, Percent change in information transmission efficiency is inversely correlated with percent change in burst rate for VPm neurons during LC activation ($r = -0.65$ and $r = -0.51$, respectively, Pearson's coefficient). **i**, Summary of TRN firing rate in response to WGN whisker stimulation under varying LC stimulation conditions. Each circle represents a TRN neuron (20.7 ± 1.9 Hz without LC stimulation vs. 20.1 ± 2.0 Hz during 2-Hz LC stimulation and vs. 18.9 ± 1.8 Hz during 5-Hz LC stimulation, $n = 22$ neurons across 10 animals, Bonferroni corrected $\alpha = 0.025$, $P = 0.54$ and $P = 0.081$, respectively, paired t test). Error bars indicate ±s.e.m.

Methods), allowed us to quantify the reliability and precision of neural responses[24]. We found that LC activation increased reliability (Fig. 5b), but not precision (Supplementary Fig. 8).

Previous work suggested that NE improves sensory processing by increasing the signal (that is, evoked responses) to noise (that is, spontaneous responses) ratio (SNR). For temporally extended stimuli, reliability is likely a more appropriate measure for SNR than the ratio of evoked to spontaneous firing rate (see Discussion). As we observed an increase in reliability with LC activation, we then examined the extent to which an increase in reliability could contribute to increases in feature selectivity and information transmission. To this end, we randomly deleted or added unreliable spikes from the VPm control spike raster until the reliability of the responses was equal to that of the responses under 5 Hz LC stimulation (see Methods). We then compared the information transmitted by the original spike train and the reliability-matched spike train. Interestingly, we found that this simulated increase in reliability only resulted in a moderate, but significant, increase in information transmission (Fig. 5a). However, this increase was drastically smaller than that observed with 5 Hz LC stimulation (that is, 469% of the control during 5 Hz LC stimulation). This suggests that LC-activation-induced increase in reliability is not likely the primary mechanism underlying the increase in thalamic information transmission.

LC modulation of thalamoreticulo–thalamic circuit dynamics improved feature selectivity and information transmission. We have demonstrated that trigeminothalamic feedforward and corticothalamic feedback input had no roles in LC modulation of thalamic information transmission (Fig. 3), indicating the locus of the mechanism underlying the observed phenomena is in the

thalamus. In the sensory thalamus, the dynamic interplay between the relay nuclei and the TRN (Fig. 5c) plays an essential role in gating information to the cortex[18,19]. The percent of spikes in bursts for VPm cells was comparable to that found in the awake somatosensory thalamus[30] (Supplementary Fig. 9a) and we found that LC activation resulted in a shift from burst to tonic firing mode for VPm neurons as both burst rate and percent of spikes in bursts decreased during LC activation (Fig. 5d and Supplementary Fig. 9b). Decreased firing rate during LC activation suggests that the suppression of VPm bursts was not simply due to the depolarizing effect of NE.

Consistent with previous work[31], we found that, during control conditions, bursting spikes carried less than half of the information carried by tonic spikes (Fig. 5e). Surprisingly, tonic spikes carried significantly more information with LC activation than without LC activation (Fig. 5e). This difference between tonic spikes with and without LC stimulation suggests a subdimension in the tonic mode, influenced by the LC, which can be modulated to allow for more efficient information transmission.

Single-unit recordings from the TRN (Fig. 5f and Supplementary Fig. 9c) revealed that LC activation also decreased TRN burst firing in response to WGN whisker stimulation, indicating an LC-activation-induced change in thalamoreticulo–thalamic circuit dynamics (Fig. 5g and Supplementary Fig. 9a,d). More interestingly, the suppression of VPm bursts was correlated with the increase in information transmission efficiency seen during LC activation (Fig. 5h). Importantly, this trend also holds in awake animals (Supplementary Fig. 10). Although LC activation reduced TRN bursting, it did not significantly alter TRN firing rate (Fig. 5i), resulting in sustained, tonic TRN inhibition being delivered to the VPm during LC activation compared with the bursting inhibition that the TRN provides without LC activation.

LC modulation of thalamic information transmission was through modulation of T-type calcium channels. We found LC activation simultaneously enhanced thalamic information transmission and reduced thalamic burst firing, which is mediated by T-type calcium channels. Yet our analyses suggested that LC-activation-improved information transmission was not simply due to VPm neurons switching from burst mode to tonic mode. However, LC regulation of intrathalamic circuit dynamics still could explain the improved tonic information transmission due to the suppressive effects of LC activation on T-type calcium channel activities involved in the subthreshold processes underlying spike generation and therefore information transmission (see Discussion).

To test the causal relationship between T-type calcium channel activity and LC-activation-induced enhancement of information transmission, we injected ML-218 hydrochloride or TTA-P2, both selective T-type calcium channel antagonists, into the thalamus to pharmacologically block these channels. Following the injection of ML-218 or TTA-P2, bursting was decreased for VPm and TRN neurons, indicating ML-218 and TTA-P2 effectively blocked calcium T-channels throughout the thalamus (Fig. 6a). Further, although LC activation had a suppressive effect on VPm and TRN burst firing in recordings before the injection of ML-218 or TTA-P2 (Fig. 6b,c), it failed to reduce burst rate following injection of ML-218 or TTA-P2 (Fig. 6b,c).

In recordings taken before ML-218 or TTA-P2 injection, we found the same LC-activity-dependent increase in feature selectivity (Fig. 6d) and enhanced thalamic information transmission efficiency (Fig. 6e). However, following the inactivation of T-type calcium channels by ML-218 and TTA-P2, we found that the LC-activity-dependent increase in feature selectivity was no longer present (Fig. 6d). Accordingly, ML-218 and TTA-P2 also blocked the LC-activity-induced increase in information transmission efficiency (Fig. 6e). The trend of LC activation effects on thalamic information transmission re-emerged after ML-218 and TTA-P2 wore off (Fig. 6d,e), indicating that the observed changes resulted from reversible pharmacological blocking of T-type calcium channels by ML-218 and TTA-P2.

Modeling confirmed that LC–NE modulation of intrathalamic circuit dynamics enhances information transmission. Isolating the effects of NE in only the VPm or TRN compared with the effects of NE in both the VPm and TRN would allow us to elucidate the mechanism behind how LC–NE modulation of intrathalamic circuit dynamics affects sensory processing. However, as it is currently technically impossible to selectively block NE effects only in the VPm or TRN in vivo due to the adjacent proximity of the VPm and TRN, we constructed a simple network model of the intrathalamic circuit (see Methods) to examine the effects of NE action in intrathalamic circuit. Thalamic neuron properties were modeled using an integrate-and-fire-or-burst (IFB) model and the effects of NE on neurotransmitter efficacy and leak current were simulated[32]. The modeled intrathalamic circuit consists of a VPm IFB neuron and a TRN IFB neuron, with the VPm neuron projecting excitatory input to the TRN neuron that provides inhibitory feedback to both the VPm neuron and itself (Fig. 7a). We used experimentally recorded PrV spike responses to WGN whisker stimulation as the input to the intrathalamic model circuit (see Methods). The spikes of the VPm model neurons could then be compared with the whisker stimulation, allowing for reverse correlation analysis and quantification of thalamic feature selectivity and information transmission of the modeled VPm neuron's outputs.

As seen in vivo, the simulated effects of NE on the modeled intrathalamic circuit resulted in an increase in feature selectivity (Fig. 7b), leading to a significant improvement in information transmission (Fig. 7c). Further, we found that the simulated effects of NE on the modeled intrathalamic circuit also resulted in the same decrease in VPm and TRN bursting rate as we observed in vivo (Fig. 7d).

Next, we used our model to investigate the effects of NE only in the VPm or only in the TRN. Simulating NE effects isolated in the VPm also resulted in an increase in information transmission (Fig. 7e); however, the increase resulting from NE effects in both VPm and TRN was significantly larger, approximately $40 \pm 16\%$, than that resulting from simulated NE effects in only the VPm ($n = 24$ features across 13 modeled VPm neurons, $\alpha = 0.05$, $P = 0.028$, paired t-test). Further, we found simulating NE effects isolated in the TRN also resulted in a slight improvement in information transmission (Fig. 7e), which was also significantly less than the improvement seen when NE affected both VPm and TRN (that is, $120 \pm 5\%$ versus $251 \pm 46\%$, $n = 24$ features across 13 modeled VPm neurons, $\alpha = 0.05$, $P = 4.7 \times 10^{-3}$, Wilcoxon signed-rank test). Although these results suggest the direct actions of NE on the VPm or TRN alone could improve thalamic information transmission, we found LC modulation of both the VPm and the TRN (that is, intrathalamic circuit dynamics) is optimal for improving thalamic feature selectivity and information transmission.

We have demonstrated in vivo that blocking T-channels in the thalamus also blocked LC modulation of thalamic information transmission, suggesting T-channels play an important role in LC–NE modulation of thalamic feature selectivity. As we hypothesized that T-current resulting from the all-or-none nature of T-channel activations is suboptimal for transmitting information about stimulus features (see Discussion), we calculated the average calcium T-channel current before spikes in our model to investigate the presumed contribution of T-channels to spike generation. As we expected, NE effects in the thalamus decreased average T-current before spikes (Fig. 7f), confirming NE improves information processing through reduction of T-channel activity as suggested by our in vivo experiments.

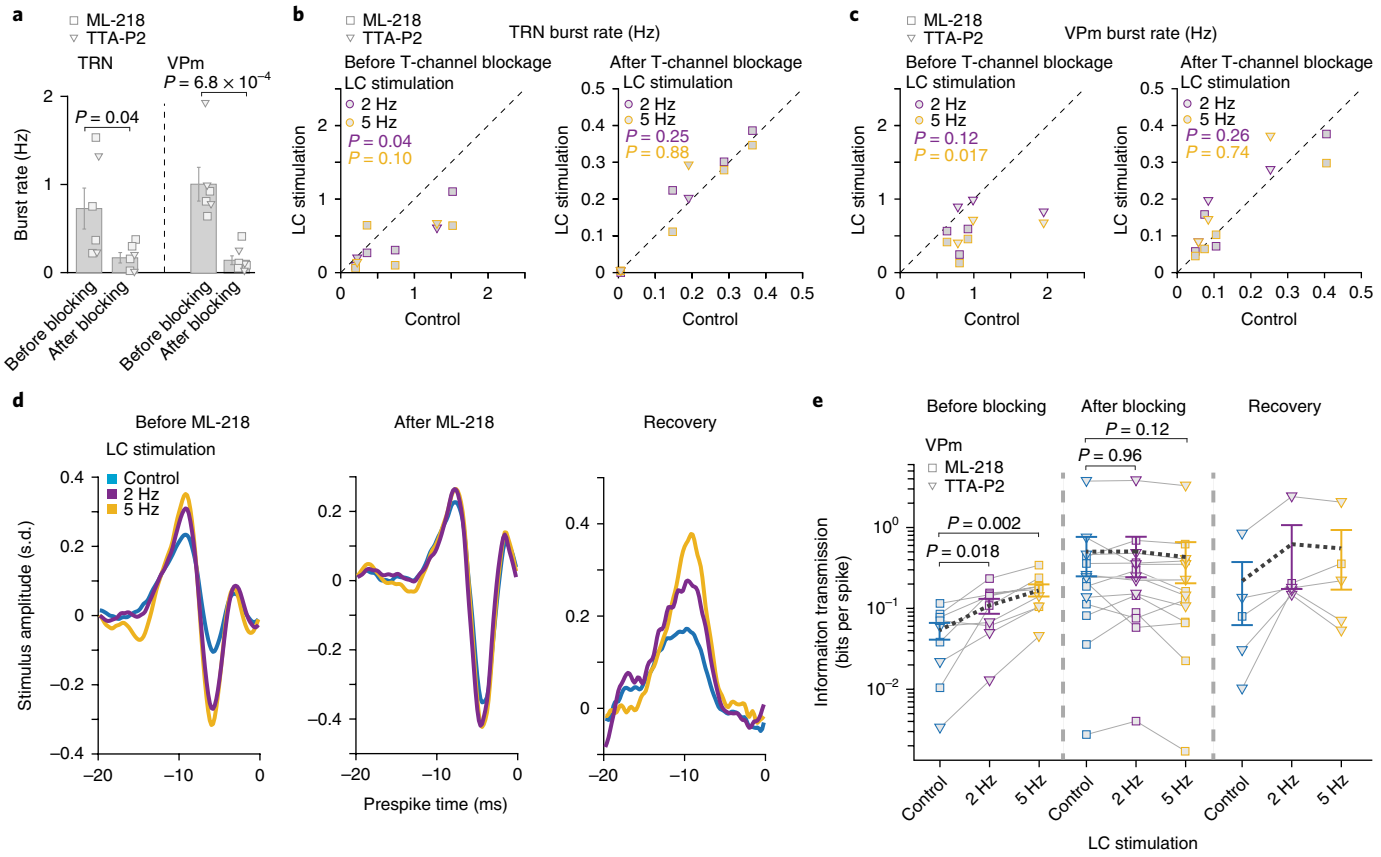

Fig. 6 | LC activation improved thalamic information transmission through modulation of T-type calcium channel activity. a, Population average of burst rate before and after ML-218 or TTA-P2 injection. Left: TRN neurons (0.73 ± 0.23 Hz before ML-218 or TTA-P2 injection vs. 0.17 ± 0.06 Hz after ML-218 injection, $n = 6$ and 6 neurons, respectively, across 5 animals, $\alpha = 0.05$, $P = 0.042$, Student's t test). Right: VPm neurons (1.02 ± 0.19 Hz before ML-218 or TTA-P2 injection vs. 0.15 ± 0.05 postinjection, $n = 6$ and 7 neurons, respectively, across 5 animals, $\alpha = 0.05$, $P = 6.8 \times 10^{-4}$, Student's t test). **b**, Summary of TRN burst rate under varying LC stimulation conditions. Left: before ML-218 or TTA-P2 injection (0.73 ± 0.23 Hz without LC stimulation vs. 0.42 ± 0.15 Hz during 2-Hz LC stimulation or 0.36 ± 0.12 Hz during 5-Hz LC stimulation, $n = 6$ neurons across 5 animals, Bonferroni corrected $\alpha = 0.025$, $P = 0.036$ and $P = 0.099$, respectively, paired t test). Right: after ML-218 or TTA-P2 injection (0.17 ± 0.06 Hz without LC stimulation vs. 0.18 ± 0.06 Hz during 2-Hz LC stimulation and vs. 0.17 ± 0.06 Hz during 5-Hz LC stimulation, $n = 6$ neurons across 5 animals, Bonferroni corrected $\alpha = 0.025$, $P = 0.25$ and $P = 0.88$, respectively, paired t test). **c**, Summary of VPm burst rate under varying LC stimulation conditions. Left: before ML-218 or TTA-P2 injection (1.02 ± 0.19 Hz without LC stimulation vs. 0.67 ± 0.11 Hz during 2-Hz LC stimulation and vs. 0.45 ± 0.08 Hz during 5-Hz LC stimulation, $n = 6$ neurons across 5 animals, Bonferroni corrected $\alpha = 0.025$, $P = 0.12$ and $P = 0.017$, respectively, paired t test). Right: after ML-218 or TTA-P2 injection (0.15 ± 0.05 Hz without LC stimulation vs. 0.17 ± 0.05 Hz during 2-Hz LC stimulation and vs. 0.16 ± 0.05 Hz during 5-Hz LC stimulation, $n = 7$ neurons across 5 animals, Bonferroni corrected $\alpha = 0.025$, $P = 0.26$ and $P = 0.74$, respectively). **d**, Example of recovered features from a VPm neuron under varying LC stimulation conditions. Left: before ML-218 injection. Center: after ML-218 injection. Right: recovery from ML-218. **e**, Population average of information transmission efficiency (bits per spike) for VPm neurons under varying LC stimulation conditions. Left: before ML-218 or TTA-P2 injection (0.05 ± 0.01 bits per spike without LC stimulation vs. 0.11 ± 0.02 bits per spike during 2-Hz LC stimulation and vs. 0.17 ± 0.03 bits per spike during 5-Hz LC stimulation, $n = 9$ features across 6 neurons across 5 animals, Bonferroni corrected $\alpha = 0.025$, $P = 0.018$ and $P = 2.3 \times 10^{-3}$, respectively, paired t test). Center: after ML-218 or TTA-P2 injection (0.51 ± 0.26 bits per spike without LC stimulation vs. 0.51 ± 0.26 bits per spike during 2-Hz LC stimulation or vs. 0.43 ± 0.23 bits per spike during 5-Hz LC stimulation, $n = 14$ features across 7 neurons across 5 animals, Bonferroni corrected $\alpha = 0.025$, $P = 0.96$ and $P = 0.12$, respectively, paired Student's t test). Right: recovery from ML-218 or TTA-P2 (~4 h after the injection, 0.22 ± 0.16 bits per spike without LC stimulation vs. 0.64 ± 0.46 bits per spike during 2-Hz LC stimulation and vs. 0.56 ± 0.39 bits per spike during 5-Hz LC stimulation, $n = 5$ features across 4 neurons across 4 animals, Bonferroni corrected $\alpha = 0.025$, $P = 0.24$ and $P = 0.22$, respectively, paired Student's t test). Each marker represents a significant feature. Error bars indicate ±s.e.m.

To elucidate the exact effects of VPm and TRN T-channels on thalamic information transmission, we removed calcium T-channels from either the VPm or TRN, or both the VPm and TRN within our model. As expected, disabling T-channels in both the VPm and TRN model neurons resulted in a dramatic improvement in information transmission (Fig. 7g). However, this improvement was not significantly different than when calcium T-channels were disabled only in the modeled VPm neuron. Further, we found that disabling calcium T-channels in only the TRN neuron resulted in a relatively small and not significant improvement in VPm information transmission (Fig. 7g).

The results from our model suggest that the main mechanism behind the experimentally observed LC–NE-induced improvement in information transmission is the reduction of calcium T-channel currents in the VPm. However, we also found that the effects of LC–NE on both the TRN and VPm in concert generate the strongest reduction in VPm calcium T-channel activity through NE's effects on intrathalamic dynamics. Taken together, these simulation results indicate that NE modulation of VPm neurons' T-channels, presumably through regulation of the interplay between the VPm and TRN, is the main source of LC-induced improvements in thalamic information transmission.

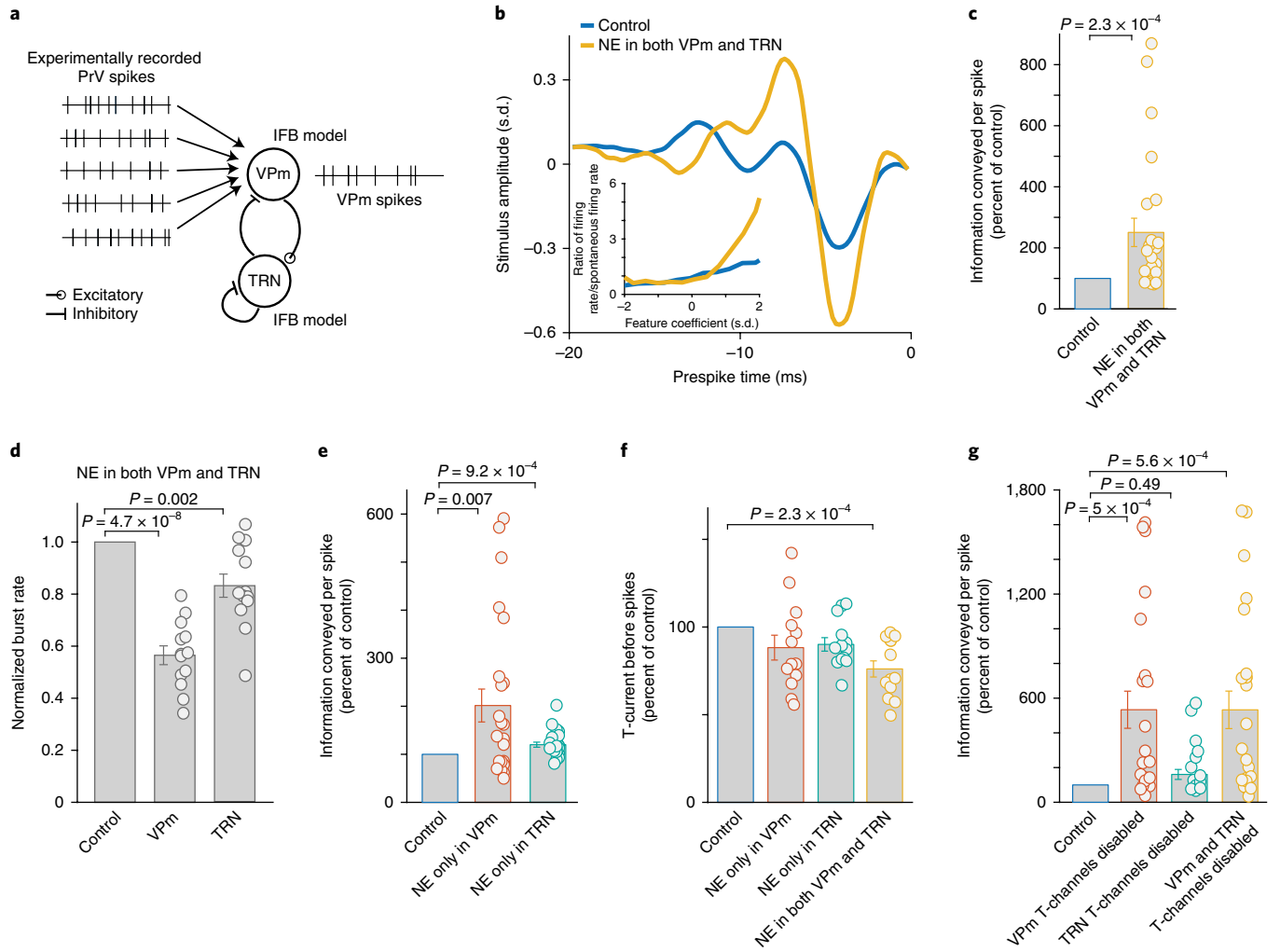

Fig. 7 | Modeling results indicated that NE action in both the VPm and TRN is optimal for enhancing thalamic information transmission. a, Diagram of the simple network model consisting of a VPm and a TRN IFB neuron. **b**, Example of recovered features of a VPm model neuron with and without NE effects on the intrathalamic circuitry. Inset: corresponding nonlinear tuning functions. **c**, Normalized changes in information transmission efficiency (bits per spike) for VPM model neurons with and without NE effects in the thalamus. Each circle represents a significant feature (251 ± 46% of the control during simulated NE effects, $n = 24$ features across 13 modeled VPm neurons, $\alpha = 0.05$, $P = 2.3 \times 10^{-4}$, Wilcoxon signed-rank test). **d**, NE action in the intrathalamic circuitry also suppressed the burst rates of both modeled VPm and TRN neurons (VPm: 56 ± 4% of control, TRN: 83 ± 4% of control, $n = 13$ modeled VPm and TRN neurons, Bonferroni corrected $\alpha = 0.025$, $P = 4.7 \times 10^{-8}$ and $P = 2.4 \times 10^{-3}$, respectively, paired t test). **e**, Normalized changes in information transmission efficiency (bits per spike) for VPM model neurons when NE only affects the VPm or TRN. Each circle represents a significant feature (202 ± 34% of the control during simulated NE effects on VPm only, 120 ± 5% of the control during simulated NE effects on TRN only, $n = 24$ features across 13 modeled VPm neurons, Bonferroni corrected $\alpha = 0.025$, $P = 6.9 \times 10^{-3}$ and $P = 9.2 \times 10^{-4}$, respectively, paired t test). **f**, Normalized T-current contributing to VPm spikes when NE acts in VPm, TRN, or both VPm and TRN (88 ± 7% of control for NE in VPm, 90 ± 4% of control for NE in TRN, 76 ± 5% of control for NE in both VPm and TRN, $n = 13$ modeled VPm neurons, Bonferroni corrected $\alpha = 0.016$, $P = 0.12$, $P = 0.024$, and $P = 2.3 \times 10^{-4}$, respectively, paired t test). **g**, Normalized changes in information transmission efficiency (bits per spike) for modeled VPm neurons when T-type Ca^{2+} channels were disabled in VPm, TRN, or both VPm and TRN (VPm T-type channels disabled: 533 ± 107%, TRN T-type channels disabled: 160 ± 29% of control, VPm and TRN T-type channels disabled: 533 ± 108% of control, $n = 24$ features across 13 modeled VPM neurons, Bonferroni corrected $\alpha = 0.016$, $P = 5.0 \times 10^{-4}$, $P = 0.49$, and $P = 5.6 \times 10^{-4}$, respectively, paired t test, Wilcoxon signed-rank test, and paired t test, respectively). Each circle represents a significant feature. Error bars indicate ±s.e.m.

LC photostimulation improved behavioral performance in tactile discrimination tasks through LC–NE optimization of thalamic sensory processing. To examine whether LC-stimulation-induced increases in information transmission by thalamic relay neurons are relevant to sensory behavior, we trained five head-fixed rats, whose LC's were selectively transfected with lentivirus to express ChR2, to perform a tactile discrimination task using a 'go'/'no-go' discrimination paradigm (Fig. 8a and Methods). Their behavioral performance with and without optogenetic LC stimulation was analyzed. During the task, the rats were required to respond (by licking) to a go stimulus (8 Hz whisker deflection) for a water reward, and withhold responses to a no-go stimulus (4 Hz whisker deflection for 2 animals; 4 and 6 Hz whisker deflection for 3 animals) to avoid a time-out period (Fig. 8b). During these training sessions, the animals were competent in performing the task, evidenced by their significantly higher probability of response to the go stimulus versus the no-go stimulus under control conditions (Fig. 8c,d).

Photostimulation of the LC resulted in a significant increase in hit rate, a slight decrease in false alarm rate associated with the 6 Hz distractor, and no change in false alarm rate associated with

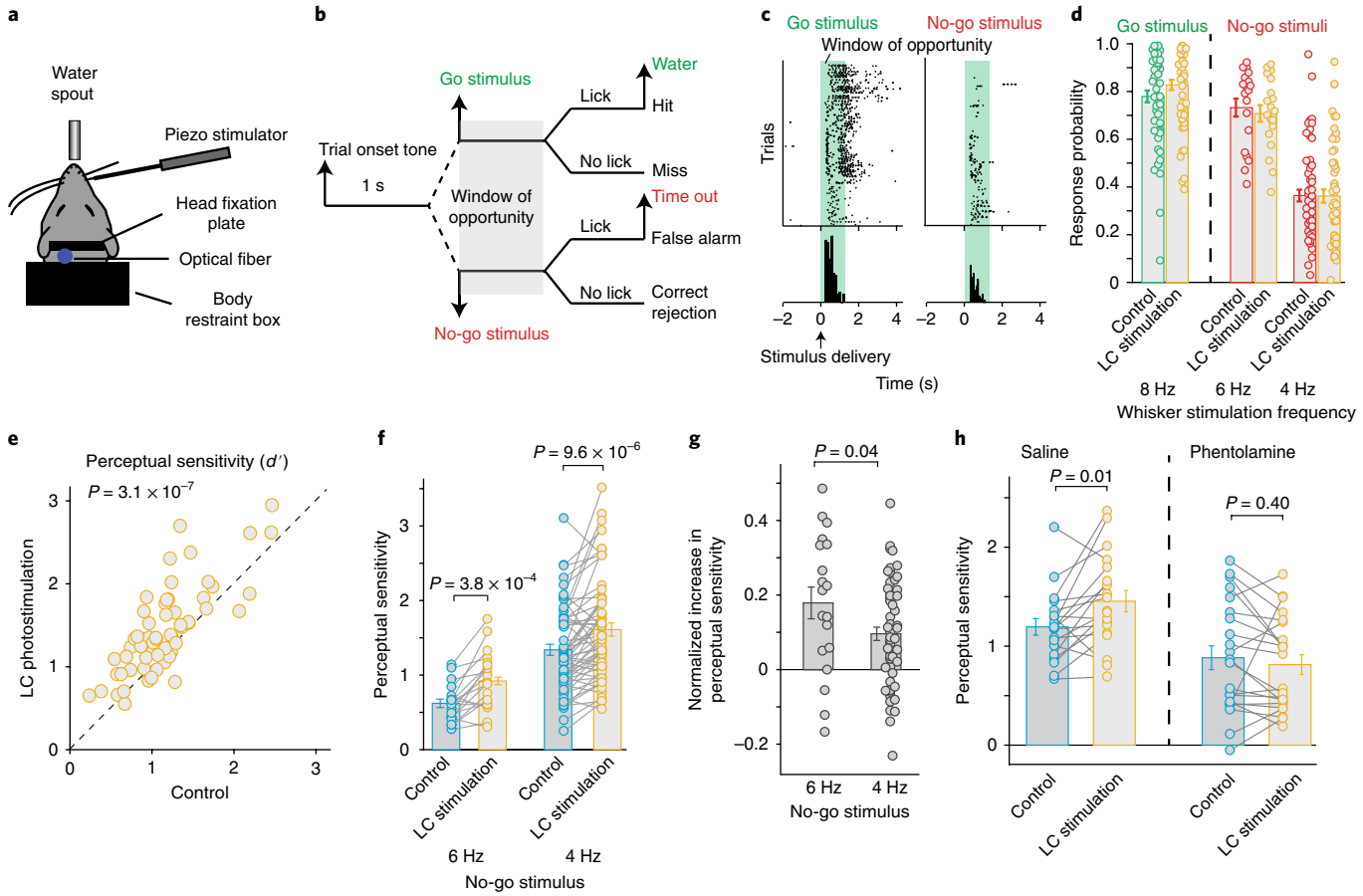

Fig. 8 | Photostimulation of LC improved behavioral performance in tactile discrimination tasks through LC–NE optimization of thalamic sensory processing. a, Schematic of the head-fixed setup. **b**, Go/no-go discrimination experiment. **c**, Example licking responses of a rat to go and no-go stimuli. Each dot represents a lick. **d**, Population average of response probability to go and no-go stimuli for rats performing the tactile discrimination task with and without LC photostimulation (hit rate: 0.78 ± 0.03 without LC stimulation vs. 0.83 ± 0.02 with LC stimulation, $n = 59$ sessions across 5 animals, $\alpha = 0.05$, $P = 1.8 \times 10^{-5}$, paired t test; response rate to 6-Hz no-go stimulus: 0.73 ± 0.04 without LC stimulation vs. 0.71 ± 0.04 with LC stimulation, $n = 19$ sessions across 3 animals, $\alpha = 0.05$, $P = 0.34$, paired t test; response rate to 4-Hz no-go stimulus: 0.36 ± 0.03 without LC stimulation vs. 0.36 ± 0.03 with LC stimulation, $n = 59$ sessions across 5 animals, $\alpha = 0.05$, $P = 0.88$, paired t test). **e**, Summary of perceptual sensitivity (d') for rats performing the tactile discrimination task, plotted for control vs. LC photostimulation conditions (1.17 ± 0.06 without LC stimulation vs. 1.43 ± 0.07 with LC stimulation, $n = 59$ sessions across 5 animals, $\alpha = 0.05$, $P = 3.1 \times 10^{-7}$, paired t test). **f**, Summary of perceptual sensitivity when discriminating between go stimulus and different no-go stimuli with and without LC photostimulation (6-Hz no-go stimulus: 0.62 ± 0.06 without LC stimulation vs. 0.92 ± 0.09 with LC stimulation, $n = 19$ sessions across 3 animals, $\alpha = 0.05$, $P = 3.8 \times 10^{-4}$, paired t test; 4-Hz no-go stimulus: 1.34 ± 0.07 without LC stimulation vs. 1.61 ± 0.09 with LC stimulation, $n = 59$ sessions across 5 animals, $\alpha = 0.05$, $P = 9.6 \times 10^{-6}$, paired t test). **g**, Normalized increase in perceptual sensitivity by LC photostimulation is greater for less discriminable no-go stimuli (0.18 ± 0.04 for 6-Hz no-go stimulus vs. 0.10 ± 0.02 for 4-Hz no-go stimulus, $n = 19$ sessions across 3 animals and 59 sessions across 5 animals, respectively, $\alpha = 0.05$, $P = 0.04$, Student's t test). **h**, Infusion of phentolamine in the thalamus blocked the LC-activation-induced improvement in perceptual sensitivity (0.88 ± 0.12 without LC stimulation vs. 0.81 ± 0.10 with LC stimulation, $n = 22$ sessions across 3 animals, $\alpha = 0.05$, $P = 0.40$, paired t test) while saline had no effect (1.19 ± 0.08 without LC stimulation vs. 1.45 ± 0.11 with LC stimulation, $n = 19$ sessions across 3 animals, $\alpha = 0.05$, $P = 0.012$, paired t test). Error bars indicate ±s.e.m.

the 4 Hz distractor (Fig. 8d). To quantify the perceptual effects of LC stimulation, we computed the rats' perceptual sensitivity (d') for each session (see Methods). We found LC stimulation significantly improved the perceptual sensitivity of these rats (Fig. 8e). Interestingly, when comparing discriminability of different no-go stimuli, the amount of significant increase in perceptual sensitivity of the rats when discriminating between 8 Hz target and 6 Hz distractor was larger than discriminating between 8 Hz target and 4 Hz distractor despite the smaller d' associated with the 6 Hz distractor (Fig. 8f). We calculated normalized increase in perceptual sensitivity (see Methods) for both distractors to take the different baseline d' values into account. The normalized increase in perceptual sensitivity for the 6 Hz distractor was significantly greater than that for the 4 Hz distractor (Fig. 8g), indicating LC stimulation is most beneficial when discriminating between stimuli with closely similar features.

These findings strongly suggest that LC-activation-induced enhancement of information transmission in the thalamic stage of the tactile pathway is beneficial for tactile discrimination of features. To conclusively determine LC-induced improvement in thalamic information processing was the causal force behind the observed increase in perceptual performance by LC activation, on a subset of experiments, we infused either phentolamine (to block NE action) or saline (as a control) into the thalamus before behavioral tasks (see Methods). Consistent with findings from our acute setup, infusion of phentolamine into the awake thalamus completely blocked the effect of LC activation on perceptual sensitivity compared to saline controls (Fig. 8h). This confirmed LC modulation of thalamic

sensory processing plays an essential role in the observed LC-induced improvement in behavioral performance for the sensory discrimination task.

Discussion

Elevated LC activity has been associated with increased arousal and an attentive behavioral state[10,28]. The LC is the primary source of adrenergic projections to the forebrain[9] and innervates the sensory pathways, suggesting a role in state-dependent modulation of sensory processing and perception. Through direct activation of the LC–NE system, we found that elevated LC–NE activity causes a dramatic increase in thalamic feature selectivity and improvement in information transmission.

Our results strongly suggest that LC-activation-induced improvement of thalamocortical information transmission is primarily mediated by NE regulation of intrathalamic circuit dynamics via the direct action of NE on α-adrenergic receptors in both the VPm and TRN. LC activation improved thalamic information transmission in both anesthetized and awake animals, suggesting that LC–NE improvement of thalamic information transmission is a general phenomenon. However, the improvement in information transmission was significantly greater in anesthetized than awake animals, likely due to the interplay in awake animals between the LC–NE system and other arousal-contributing neuromodulators, which are probably more active in the waking state[13,14,33,34]. Importantly, we found photostimulation of the LC in awake, head-fixed rats improved behavioral performance on a perceptual discrimination task and this enhancement of behavior was due to NE regulation of intrathalamic circuit dynamics. This suggests LC modulation of sensory processing in the early stage of sensory pathways is critical to perception.

Recent studies have demonstrated that LC activation elicits frequency-dependent pupil dilation[23,35]. Taken together, these results and our results presented here are consistent with several previous studies that have shown a relationship between pupil size and sensory processing[5–7]. While these previous studies have demonstrated that pupil-linked arousal, presumably mediated by the LC–NE system, is tightly correlated with improved cortical encoding of sensory signals, our data suggest that pupil-linked improvement in sensory processing could already occur in first-order thalamic neurons.

Alert, aroused states and locomotion have both been linked to increased neuronal response to sensory input[3–5,36], indicating gain increases with heightened behavioral states. This increased responsiveness, however, did not alter sensory neurons' sensitivity to stimuli[3,36]. We found LC activation decreased the overall response of VPm neurons to continuous whisker stimulation. Surprisingly, this decreased gain was coupled with a drastic improvement in information transmission that cannot be explained by the reduction in gain (Fig. 5a). Our isolation of the effects of the LC–NE system may lend an explanation for this surprising result. In awake, behaving animals, behavioral state is modulated by a complex interplay between multiple neuromodulatory systems, including the noradrenergic and cholinergic systems[13,33]. Indeed, activation of either the LC or the cholinergic basal forebrain desynchronizes cortical electroencephalogram[23,37]. Cholinergic system activation increases firing rate for neurons in the visual cortex[38], suggesting that cholinergic systems may potentially counterbalance the suppressive effects of the LC–NE system observed in this study. Indeed, the cholinergic system is activated by locomotion and plays a role in locomotion-linked visual sensory processing[39,40]. Our findings are, nevertheless, consistent with the notion that norepinephrine boosts the effective salience of incoming sensory signals[9,11]. Increased selectivity of the response of thalamocortical neurons during LC-mediated arousal may provide the cortex with a more accurate representation of stimuli. This may lead to more effective functional reorganization of cortical representation of behaviorally important sensory signals, possibly through noradrenergic plasticity in concert with other top-down/bottom-up mechanisms[1,16,29].

Local application of norepinephrine in the somatosensory thalamus has been shown to suppress spontaneous activity while slightly increasing isolated-punctate-whisker-deflection-evoked responses, resulting in an increased SNR, defined as the ratio of evoked to spontaneous firing rate[34]. This led to an NE-induced increase in SNR to be initially hypothesized as the mechanism underlying LC-activity-induced improved thalamic sensory processing. Most complex sensory guided behavior involves naturalistic, temporally extended stimuli (for example, whisking against a textured surface), for which evoked and spontaneous spikes cannot be easily identified; however, reliability can be used as a measure of SNR for these responses[24]. During continuous whisker stimulation, reliable and unreliable spikes are analogous to evoked and spontaneous spikes, respectively, as reliable spikes carry significantly more stimulus-related information than unreliable spikes (data not shown). Although LC activation increased the reliability of thalamic responses, we found increased SNR, as measured by reliability, could not explain the drastically improved thalamocortical encoding (Fig. 5a).

Previous work has shown thalamic relay neurons fire in two modes: tonic and bursting[41,42]. Although burst firing is shown to be present in the awake thalamus[30,43,44], it is believed to serve as a 'wake-up call' to the cortex. Tonic mode, in contrast, is thought to be more ideal for transmission of detailed information about stimuli[31]. When de-inactivated, a weak incoming excitatory postsynaptic potential (EPSP) could activate T-type calcium channels to generate powerful low-threshold calcium spikes, which in turn trigger sodium spikes[41,42]. This all-or-none nature of T-channel activation may result in VPm spikes that are less selective to a specific encoded feature as due to the facilitative action of T-channels, weak EPSPs from non-encoded features could produce the same spiking activity as strong EPSPs produced by encoded features.

During low arousal, thalamic neurons are relatively hyperpolarized[14], which increases the likelihood of T-type calcium channels being de-inactivated. Due to the reciprocal connection between the VPm and TRN, a burst of TRN spikes has been shown to hyperpolarize thalamocortical neurons, and thus increase the portion of de-inactivated T-channels, indicated by increases in burst firing[45]. TRN neurons also exhibit a stereotyped after-burst hyperpolarization lasting ~100–120 ms (ref. [46]). This hyperpolarization is long enough to de-inactivate T-type calcium channels in the TRN, enabling TRN neurons to burst again after a moderate depolarization resulting from VPm spikes. Larger fluctuations of VPm membrane potential caused by this bursting activity within the thalamoreticulo–thalamic circuitry may increase the portion of time T-channels are de-inactivated, which would be detrimental to unbiased, linear transformation of feedforward PrV synaptic inputs to suprathreshold activity. In line with this notion, our experimental and simulation data demonstrated the detrimental role of T-type calcium channel activity to information transmission as blocking T-type calcium channels drastically improved information transmission (Figs. 6 and 7).

Our data showed that LC activation reduced bursting for VPm neurons, which, at first glance, suggested that the observed LC-activation-improved information transmission was merely a result of an LC-induced switch to a tonic firing mode. However, to our surprise, further analyses showed that this is not the case, as information carried by tonic spikes with LC stimulation was approximately threefold that of tonic spikes from the same VPm neuron without LC stimulation (Fig. 5e), suggesting that tonic mode during LC activation was not functionally equivalent to tonic mode without LC activation.

What then is the difference between the tonic mode with and without LC stimulation? An explanation to why tonic spikes during LC activation are more informative may come from a recent

finding that a small portion of T-type channels are de-inactivated even during relatively depolarized states[47]. Although small, due to the strength of T-type channel conductance, this population may still significantly contribute to tonic spiking. These results showed graded activation of T-channels facilitated the generation of tonic spikes, and improved the input–output gain of thalamic relay neurons, presumably making them more optimal for detecting sensory input than discriminating between different features within the sensory input[17,47]. During LC activation, NE altered intrathalamic circuit dynamics, which resulted in steady TRN tonic inhibition of the VPm (Fig. 5g). VPm neurons then experienced both the steady depolarizing effects of NE and the tonic hyperpolarizing effects of TRN inhibition, perhaps creating concurrent push–pull forces on membrane potential that may buffer against fluctuations[13]. As previous experimental evidence has suggested that even short periods of hyperpolarization have statistically significant effects on recruiting more T-channels in thalamocortical cells[48], the collective effects described above likely diminish the overall contribution of T-channel current to tonic spikes, thus improving information transmission about the encoded features.

In support of this notion, recent studies showed a reduction in the variance of membrane potential during high arousal indexed by pupil size and locomotion[5,36,49]. Consistent with these previous studies, our modeling results showed a decrease in the variance of VPm membrane potential during simulated NE action in the thalamus (Supplementary Fig. 11a). Further, our in vivo data demonstrated a decrease in the coefficient of variance of inter-spike intervals during LC activation (Supplementary Fig. 11b), quantitatively indicating a decrease in fluctuation of VPm membrane potential during LC activation[50]. Therefore, we suggest a new brain-state-dependent subdimension within the tonic mode, in which the LC, and perhaps other neuromodulatory systems, can optimize thalamocortical information transmission through modulating intrathalamic circuit dynamics. Future studies combining whole-cell recording and LC manipulation are necessary to definitively test this potential cellular mechanism.

Online content

Any methods, additional references, Nature Research reporting summaries, source data, statements of data availability and associated accession codes are available at https://doi.org/10.1038/s41593-018-0283-1.

Received: 18 January 2018; Accepted: 1 November 2018;
Published online: 17 December 2018

References

1. Briggs, F., Mangun, G. R. & Usrey, W. M. Attention enhances synaptic efficacy and the signal-to-noise ratio in neural circuits. *Nature* **499**, 476–480 (2013).
2. Poulet, J. F. A. & Petersen, C. C. H. Internal brain state regulates membrane potential synchrony in barrel cortex of behaving mice. *Nature* **454**, 881–885 (2008).
3. Cano, M., Bezdudnaya, T., Swadlow, H. A. & Alonso, J.-M. Brain state and contrast sensitivity in the awake visual thalamus. *Nat. Neurosci.* **9**, 1240–1242 (2006).
4. Niell, C. M. & Stryker, M. P. Modulation of visual responses by behavioral state in mouse visual cortex. *Neuron* **65**, 472–479 (2010).
5. Reimer, J. et al. Pupil fluctuations track fast switching of cortical states during quiet wakefulness. *Neuron* **84**, 355–362 (2014).
6. McGinley, M. J., David, S. V. & McCormick, D. A. Cortical membrane potential signature of optimal states for sensory signal detection. *Neuron* **87**, 179–192 (2015).
7. Vinck, M., Batista-Brito, R., Knoblich, U. & Cardin, J. A. Arousal and locomotion make distinct contributions to cortical activity patterns and visual encoding. *Neuron* **86**, 740–754 (2015).
8. Scholvinck, M. L., Saleem, A. B., Benucci, A., Harris, K. D. & Carandini, M. Cortical state determines global variability and correlations in visual cortex. *J. Neurosci.* **35**, 170–178 (2015).
9. Sara, SusanJ. & Bouret, S. Orienting and reorienting: the locus coeruleus mediates cognition through arousal. *Neuron* **76**, 130–141 (2012).
10. Aston-Jones, G. & Cohen, J. D. An integrative theory of locus coeruleus-norepinephrine function: adaptive gain and optimal performance. *Annu. Rev. Neurosci.* **28**, 403–450 (2005).
11. Usher, M., Cohen, J. D., Servan-Schreiber, D., Rajkowski, J. & Aston-Jones, G. The role of locus coeruleus in the regulation of cognitive performance. *Science* **283**, 549–554 (1999).
12. Devilbiss, D. M., Page, M. E. & Waterhouse, B. D. Locus ceruleus regulates sensory encoding by neurons and networks in waking animals. *J. Neurosci.* **26**, 9860–9872 (2006).
13. McGinley, M. J. et al. Waking state: rapid variations modulate neural and behavioral responses. *Neuron* **87**, 1143–1161 (2015).
14. Steriade, M., McCormick, D. A. & Sejnowski, T. J. Thalamocortical oscillations in the sleeping and aroused brain. *Science* **262**, 679–685 (1993).
15. Guo, Z. V. et al. Maintenance of persistent activity in a frontal thalamocortical loop. *Nature* **545**, 181–186 (2017).
16. Wang, H.-P., Spencer, D., Fellous, J.-M. & Sejnowski, T. J. Synchrony of thalamocortical inputs maximizes cortical reliability. *Science* **328**, 106–109 (2010).
17. Wang, Q., Webber, R. & Stanley, G. B. Thalamic synchrony and the adaptive gating of information flow to cortex. *Nat. Neurosci.* **13**, 1534–1541 (2010).
18. Wimmer, R. D. et al. Thalamic control of sensory selection in divided attention. *Nature* **526**, 705–709 (2015).
19. Crick, F. Function of the thalamic reticular complex: the searchlight hypothesis. *Proc. Natl Acad. Sci. USA* **81**, 4586–4590 (1984).
20. Petersen, R. S. et al. Diverse and temporally precise kinetic feature selectivity in the VPm thalamic nucleus. *Neuron* **60**, 890–903 (2008).
21. Jadhav, S. P., Wolfe, J. & Feldman, D. E. Sparse temporal coding of elementary tactile features during active whisker sensation. *Nat. Neurosci.* **12**, 792–800 (2009).
22. Vaingankar, V., Soto-Sanchez, C., Wang, X., Sommer, F. T. & Hirsch, J. A. Neurons in the thalamic reticular nucleus are selective for diverse and complex visual features. *Front. Integr. Neurosci.* **6**, 118 (2012).
23. Liu, Y., Rodenkirch, C., Moskowitz, N., Schriver, B. & Wang, Q. Dynamic lateralization of pupil dilation evoked by locus coeruleus activation results from sympathetic, not parasympathetic, contributions. *Cell Rep.* **20**, 3099–3112 (2017).
24. Mainen, Z. F. & Sejnowski, T. J. Reliability of spike timing in neocortical neurons. *Science* **268**, 1503–1506 (1995).
25. Adelman, T. L., Bialek, W. & Olberg, R. M. The information content of receptive fields. *Neuron* **40**, 823–833 (2003).
26. Abbott, S. B. G., Stornetta, R. L., Socolovsky, C. S., West, G. H. & Guyenet, P. G. Photostimulation of channelrhodopsin-2 expressing ventrolateral medullary neurons increases sympathetic nerve activity and blood pressure in rats. *J. Physiol.* **587**, 5613–5631 (2009).
27. Crandall, S. R., Cruikshank, S. J. & Connors, B. W. A corticothalamic switch: controlling the thalamus with dynamic synapses. *Neuron* **86**, 768–782 (2015).
28. Berridge, C. W. & Waterhouse, B. D. The locus coeruleus–noradrenergic system: modulation of behavioral state and state-dependent cognitive processes. *Brain. Res. Rev.* **42**, 33–84 (2003).
29. Martins, A. R. O. & Froemke, R. C. Coordinated forms of noradrenergic plasticity in the locus coeruleus and primary auditory cortex. *Nat. Neurosci.* **18**, 1483–1492 (2015).
30. Ramcharan, E. J., Gnadt, J. W. & Sherman, S. M. Burst and tonic firing in thalamic cells of unanesthetized, behaving monkeys. *Vis. Neurosci.* **17**, 55–62 (2000).
31. Reinagel, P., Godwin, D., Sherman, S. M. & Koch, C. Encoding of visual information by LGN bursts. *J. Neurophysiol.* **81**, 2558–2569 (1999).
32. Moxon, K. A., Devilbiss, D. M., Chapin, J. K. & Waterhouse, B. D. Influence of norepinephrine on somatosensory neuronal responses in the rat thalamus: A combined modeling and in vivo multi-channel, multi-neuron recording study. *Brain Res.* **1147**, 105–123 (2007).
33. Harris, K. D. & Thiele, A. Cortical state and attention. *Nat. Rev. Neurosci.* **12**, 509–523 (2011).
34. Hirata, A., Aguilar, J. & Castro-Alamancos, M. A. Noradrenergic activation amplifies bottom-up and top-down signal-to-noise ratios in sensory thalamus. *J. Neurosci.* **26**, 4426–4436 (2006).
35. Joshi, S., Li, Y., Kalwani, Rishi M. & Gold, Joshua I. Relationships between pupil diameter and neuronal activity in the locus coeruleus, colliculi, and cingulate cortex. *Neuron* **89**, 221–234 (2016).
36. Polack, P. O., Friedman, J. & Golshani, P. Cellular mechanisms of brain state-dependent gain modulation in visual cortex. *Nat. Neurosci.* **16**, 1331–1339 (2013).
37. Goard, M. & Dan, Y. Basal forebrain activation enhances cortical coding of natural scenes. *Nat. Neurosci.* **12**, 1444–1449 (2009).
38. Pinto, L. et al. Fast modulation of visual perception by basal forebrain cholinergic neurons. *Nat. Neurosci.* **16**, 1857–1863 (2013).
39. Fu, Y. et al. A cortical circuit for gain control by behavioral state. *Cell* **156**, 1139–1152 (2014).

40. Lee, A. M. et al. Identification of a brainstem circuit regulating visual cortical state in parallel with locomotion. *Neuron* **83**, 455–466 (2014).
41. Sherman, S. M. Tonic and burst firing: dual modes of thalamocortical relay. *Trends Neurosci.* **24**, 122–126 (2001).
42. Llinas, R. & Jahnsen, H. Electrophysiology of mammalian thalamic neurones in vitro. *Nature* **297**, 406–408 (1982).
43. Fanselow, E. E., Sameshima, K., Baccala, L. A. & Nicolelis, M. A. Thalamic bursting in rats during different awake behavioral states. *Proc. Natl Acad. Sci. USA* **98**, 15330–15335 (2001).
44. Swadlow, H. A. & Gusev, A. G. The impact of 'bursting' thalamic impulses at a neocortical synapse. *Nat. Neurosci.* **4**, 402–408 (2001).
45. Halassa, M. M. et al. Selective optical drive of thalamic reticular nucleus generates thalamic bursts and cortical spindles. *Nat. Neurosci.* **14**, 1118–1120 (2011).
46. Avanzini, G., de Curtis, M., Panzica, F. & Spreafico, R. Intrinsic properties of nucleus reticularis thalami neurones of the rat studied in vitro. *J. Physiol.* **416**, 111–122 (1989).
47. Deleuze, C. et al. T-type calcium channels consolidate tonic action potential output of thalamic neurons to neocortex. *J. Neurosci.* **32**, 12228–12236 (2012).
48. Wolfart, J., Debay, D., Le Masson, G., Destexhe, A. & Bal, T. Synaptic background activity controls spike transfer from thalamus to cortex. *Nat. Neurosci.* **8**, 1760–1767 (2005).
49. Bennett, C., Arroyo, S. & Hestrin, S. Subthreshold mechanisms underlying state-dependent modulation of visual responses. *Neuron* **80**, 350–357 (2013).
50. Stern, E. A., Kincaid, A. E. & Wilson, C. J. Spontaneous subthreshold membrane potential fluctuations and action potential variability of rat corticostriatal and striatal neurons in vivo. *J. Neurophysiol.* **77**, 1697–1715 (1997).

Acknowledgements

We thank J. M. Alonso for comments at various points of this work and R. L. Stornetta for sharing lentiviral vectors with us. This work was supported by the National Institutes of Health (NIH R01MH112267 to Q.W.).

Author contributions

Q.W. and C.R. designed the project. C.R, Y.L., and Q.W. performed in vivo experiments. C.R. analyzed the data and performed modeling with Q.W.'s guidance. B.J.S. performed and analyzed behavioral experiments. Q.W. supervised the entire project. Q.W. and C.R. wrote the manuscript with input from Y.L and B.J.S.

Competing interests

The authors declare no competing interests.

Additional information

Supplementary information is available for this paper at https://doi.org/10.1038/s41593-018-0283-1.

Reprints and permissions information is available at www.nature.com/reprints.

Correspondence and requests for materials should be addressed to Q.W.

Publisher's note: Springer Nature remains neutral with regard to jurisdictional claims in published maps and institutional affiliations.

Methods

Surgery. All procedures performed on animals were approved by the Institutional Animal Care and Use Committees at Columbia University, and were conducted in compliance with guidelines of the National Institutes of Health. Adult female Sprague–Dawley rats weighing between 225 and 300 g (Charles River Laboratories) were used.

Acute procedures were similar to those described previously[17,23]. Briefly, rats were sedated with 5% vaporized isoflurane in the home cages before being transported to the surgery suite. Once mounted on a stereotaxic frame, the anesthetic was switched to sodium pentobarbital (intravenously through tail vein, initial dose 30 mg kg^{-1}), which was maintained throughout the surgery via a syringe pump. Body temperature was maintained at 37 °C by a servo-controlled heating pad and blood-oxygen saturation level and heart rate were continuously monitored. To allow for placement of a microelectrode within the LC, a small craniotomy was made over the left LC. A second craniotomy was then created above either the PrV, VPm, or TRN representing the right whiskers to allow for recording. On a subset of surgeries, a third craniotomy was made to allow access to the left barrel cortex. Any exposed brain surface was then covered in warm saline, contained by retaining wells created around the craniotomies.

Electrophysiology. Single, sharp tungsten microelectrodes (75 µm in diameter, impedance of ~3 MΩ, FHC) were used to record extracellular single-unit activity. Extracellular neural signals were referenced to a ground screw in contact with the dura, band-pass filtered (300–8,000 Hz), and digitized at 40 kHz using a Plexon recording system (OmniPlex, Plexon). Spike sorting of single units was performed using commercially available software (Offline Sorter, Plexon). Only large, easily isolatable units with a minimum refractory period greater than 1 ms and a stable waveform throughout the entire recording were used. A hydraulic micropositioner (David Kopf) allowed for slow, controlled positioning of the electrode adjacent to recorded neurons.

Identification of LC neurons has been described in detail previously[23], and was based on LC neuron hallmarks: wide action potential waveform (>1.8 ms) and elevated firing rate in response to paw or tail pinch followed by a brief suppression period (Fig. 1b). VPm neurons were verified by their depth (greater than 5 mm), response to a half-sinusoid whisker deflection (10 ms duration), and ability to continuously respond to continuous whisker stimulation[17]. When recording from the PrV, to ensure we did not accidently record from the caudally adjacent SpV, the initial penetration was done rostral of the PrV (~3 mm caudal to lambda), then subsequent penetrations were performed, moving 100 µm posterior between each penetration, until neurons responding to whisker stimulation were found, thus ensuring we were recording from the rostral edge of the PrV, located away from the SpV[51]. PrV identity was further confirmed by short-latency response to a half-sinusoid whisker deflection (Supplementary Fig. 5a). TRN neurons were identified by their narrow waveform, and response to a half-sinusoid whisker deflection (Supplementary Fig. 9c). Barrel cortex columns were mapped based on responses to manual stimulation of individual whiskers.

Following completion of the experiment, in a subset of experiments for each recorded location, the recording system was disconnected and an electrical microstimulator (Multi Channel Systems) was used to pass a DC current (200 µA, 10 s) through the stimulating electrode, at points located every 500 µm during retraction, which created lesions visible in histology. The animal was subsequently transcardially perfused with 4% paraformaldehyde, and the brain was collected for post-experiment histological analysis, allowing the recording location to be further confirmed.

LC activation. After electrophysiologically confirming the microelectrode was within the LC, the electrode was disconnected from the recording system and connected to a calibrated electrical microstimulator (S88, Grass Instrument), which was then triggered by a xPC target real-time system (Mathworks) running at 1 kHz. During periods of microstimulation-induced LC activation, cathode-leading biphasic current pulses (200 µs per phase, 60 µA) were continuously delivered at either 2 or 5 Hz, beginning 5 s before whisker stimulation and lasting throughout the entire period of whisker stimulation for a total length of 165 s. Ninety-five seconds of dead time was inserted between each stimulation period to allow for the system to return to baseline conditions. For each recording, 3–13 repetitions (average 5.64 ± 0.62 repetitions) of each LC condition were delivered in a random order.

For optogenetic LC activation, during the initial aseptic surgery, a craniotomy was created above the LC and the LC was mapped using the stereotaxic coordinates and electrophysiological characteristics listed above. We then injected a lentivirus, which selectively transfects noradrenergic LC neurons, resulting in these neurons expressing ChR2 (pLenti-PRSx8-hChR2(H134R)-mCherry, the UNC vector core, ~7×10^9 vp ml^{-1}). The virus was injected through a pulled glass pipette using a pico-injector (PLI100, Harvard Apparatus, 100 nl min^{-1}). Four weeks following the initial injection, a second surgery was performed during which a fiber optic cannula (200 µm diameter, 0.39 NA) was positioned targeting the LC. Animals that were to be used for chronic recordings had the fiber optic cannula affixed in place, along with a metal plate to allow for head fixation, using dental cement and bone screws anchored around the perimeter of the skull. These animals were given a four-week recovery period before being used for behavioral training. Animals that were used for acute recordings had the fiber optic cannula simply held in place using a micropositioner, and the acute experiments were performed directly after insertion of the fiber optic cannula. This transfection and fiber optic cannula implantation allowed us to selectively activate the LC using photostimulation (493 nm wavelength). LC stimulation patterns were identical to those used with electrical microstimulation, with the biphasic current pulse simply replaced by a pulse of blue light (20 mW mm^{-2}, pulse length 5 ms).

Whisker stimulation. A custom-modified galvomotor (galvanometer optical scanner model 6210 H, Cambridge Technologies) controlled by a closed-loop system (micromax 67145 board, Cambridge Technology) was used to deliver precise, high-frequency mechanical whisker stimulations. Whiskers were cut to a length of ~10 mm, and inserted into the deflecting arm so that the arm was positioned ~5 mm from the skin. During each block of an LC stimulation condition, following a 5 s period allowing the system to adjust to the new condition, the galvomotor was used to continuously deliver whisker deflection following a signal consisting of 8 repetitions of a 20 s clip of frozen WGN. Two versions of frozen WGN were used (standard deviation of 1.4 or 1.2 degrees deflection) and both yielded similar results. All WGN was low-pass filtered (Butterworth, 10th order) at 250 Hz (Supplementary Fig. 1b). This resulted in 24–104 repetitions (average 45.09 ± 4.92) of the WGN during each LC stimulation condition per neuron.

Pharmacological manipulations. In a subset of experiments, the barrel columns of the barrel cortex were mapped. We then injected muscimol (2 µl, 5 mM, injected at 100 nl min^{-1}) directly into the center of the cortical craniotomy, through a pulled glass pipette (20 µm opening) using a pico-injector (PLI100, Harvard Apparatus). These injections silenced any responses of barrel cortex neurons, in the injected or adjacent columns, to whisker deflections as evidenced by the disappearance of an LFP response (Supplementary Fig. 6b). VPm recordings following these injections were then taken from the barreloid topographically aligned with the barrel column into which we injected muscimol, confirmed by the VPm neurons' response to the same primary whisker.

On another subset of experiments, phentolamine, an α-adrenergic receptor antagonist (~2 µl 10 mM injected at 100 nl min^{-1}), ML-218 hydrochloride, a selective inhibitor of T-type calcium channels[52] (~2 µl, dissolved in DMSO at 25 mM, diluted with saline to 5 mM, injected at 100 nl min^{-1}), TTA-P2, another selective inhibitor of T-type calcium channels[47] (~2 µl, dissolved in DMSO at 25 mM, diluted with saline to 5 mM, injected at 100 nl min^{-1}), or saline (~2 µl, as a control, injected at 100 nl min^{-1}) was directly injected into the thalamus. This was accomplished using a pulled glass pipette using a pico-injector (PLI100, Harvard Apparatus) for acute animals and through an implanted cannula targeting the thalamus for behaving animals.

Awake head-fixed electrophysiology. After recovery from the implantation of a recording window[53], animals were trained daily to tolerate head fixation until all signs of stress during head fixation disappeared (for example, teeth chattering, porphyrin staining, vocalization, and physically resisting fixation), at which point we began collecting recordings of VPm neurons in response to WGN whisker stimulus under varying levels of LC activation. The recordings were performed in a light and sound attenuation chamber.

Data analysis. Both PrV and VPm neurons can be modeled by the linear–nonlinear–Poisson model[20,54]. Therefore, by analyzing the neuron's spiking response to a repeated delivery of a frozen 20 s clip of WGN whisker deflection, we can recover the neurons' feature selectivity in terms of a linear filter set and the corresponding set of nonlinear tuning functions. Here we recovered each neuron's first significant feature using a spike triggered average (STA) to calculate the average whisker displacement in a 20 ms window preceding a spike. We then used a spike triggered covariance (STC) matrix to recover the remaining set of significant features for any neurons that selectively responded to more than one kinetic feature[20,54].

$$\mathbf{STA} = \frac{1}{N}\sum_{n=1}^{N}\mathbf{S}(t_n)$$

$$STC = \frac{1}{N-1}\sum_{n=1}^{N}[\mathbf{S}(t_n)-\mathbf{STA}]\,[\mathbf{S}(t_n)-\mathbf{STA}]^T$$

where t_n is the time of the nth spike, $\vec{S}(t_n)$ is a vector representing the stimulus during the temporal window preceding that spike, N is the total number of spikes, and $[]^T$ indicates the transpose of a matrix.

Statistical significance of STAs was determined using a bootstrap procedure (1,000 bootstrap trials). Any recovered STAs whose amplitude fell within the 99.9 percentile of the bootstrap displacement range were considered insignificant. The significance of STC recovered filters was determined using nestled bootstrapping of the eigenvalues corresponding to the STC recovered filters. If a recovered eigenvalue exceeded the 99.9 percentile of its corresponding bootstrap range its

filter was considered significant. Neurons without significant feature selectivity were excluded from further analysis.

To quantify the modulation of the recovered features by LC activation, we defined a feature modulation factor as:

$$\textit{Feature modulation factor} = \frac{\textbf{Control feature} \cdot \textbf{Conditional feature}}{\textbf{Control feature} \cdot \textbf{Control feature}}$$

Alternatively, feature amplitude was also calculated as the peak-to-peak displacement amplitude of the feature.

To estimate the nonlinear tuning functions corresponding to the significant recovered features, we calculated the feature coefficient, defined as the dot product between a neuron's linear filter and a stimulus feature, preceding each spike, from which the probability distribution of feature coefficient values k given a spike (that is, Prob(k|spike)) was generated. All possible feature coefficients were then found for the stimulus used, calculated by sliding a 20 ms window through the 20 s WGN stimulus, from which a probability distribution of all feature coefficient values (that is, Prob(k)) was generated. Then by dividing Prob(k|spike) by Prob(k), we generated the nonlinear tuning function value which maps firing rate to feature coefficient value.

To quantify the information the spike train conveys about the absence/presence of a feature under varying LC activation conditions, we calculated mutual information between the presence or absence of a feature and the observation of a spike as[20,25]:

$$Info(k; spike) = \int dk \times Prob(k \mid spike) \times \log_2\left[\frac{Prob(k \mid spike)}{Prob(k)}\right]$$

where k is the feature. Information transmission rate, that is, bits per second, was calculated by multiplying bits per spike by the average firing rate of the neuron in response to WGN stimulus.

To facilitate event-based analysis, the peristimulus time histogram of the neuron's responses was binned (2 ms bins) and convolved with an adaptive boxcar kernel[24], whose size was dynamically increased from 1 at each bin until the bins spanned by that kernel contained at least 10 spikes, to produce a SDF. Any points where the SDF crossed a threshold set at 3 times the mean firing rate was defined as an event, as previously suggested[24]. Spikes that fell within events were considered reliable while spikes outside of events were classified as unreliable spikes. Precision was calculated as the average standard deviation of spike times within each event.

Burst spiking was defined as any two or more spikes occurring with an inter-spike interval of 4 ms or less and following at least 100 ms of quiescence[41]. Coefficient of variation of inter-spike intervals was calculated as the standard deviation of inter-spike intervals divided by the mean inter-spike interval.

To test whether reduction in gain or increased reliability could explain the increase in information transmission by VPm neurons in response to LC activation, we computationally manipulated recorded spike trains. To simulate firing rate reduction, we randomly deleted spikes from the 0 Hz LC stimulation spike train, for each recording, until its firing rate matched that of the neurons 5 Hz LC stimulation spike train. To match the reliability of the recorded control VPm spike train to that of the VPm spike train with 5 Hz LC stimulation, we first calculated the reliability of the VPm spike train with 5 Hz LC stimulation. We then estimated the amount of unreliable or reliable spikes that would need to be deleted from the control VPm spike train to make its reliability match that of the 5 Hz LC stimulation VPm spike train. For the majority of recordings (18 of 22 cells), the LC 5 Hz spike train was more reliable than the control VPm spike train, and a set of random chosen unreliable spikes was deleted. However, for a minority of recordings (4 of 22) in which the 5 Hz LC stimulation spike train was less reliable than the control spike train, a randomly selected set of reliable spikes were deleted. Once the computationally modified control VPm spike train was generated, its new reliability was calculated. If the new reliability did not closely match that of the 5 Hz LC stimulation VPm spike train (as changes in event threshold produced by change in firing rate affect reliability calculations), the estimation of unreliable or reliable spikes needed to be removed was incremented or decremented as necessary and the above manipulations were again applied to the original control VPm spike train. This process was repeated until the reliability of computationally modified control spike train was accurately matched to that of the corresponding 5 Hz LC stimulation spike train. We then calculated the feature selectivity and information transmission of these reliability-matched spike trains. For each recording, the above computational manipulation was performed 1,000 times, with information transmission being calculated for each of the 1,000 simulations. The average of the resulting 1,000 information transmission values was then found and used for each recording.

Behavior. Five rats were used for behavior. ChR2 was expressed in the left LC using the lentiviral vector (see 'LC activation'). All animals were implanted with an optical fiber targeting the left LC and a head plate. Three animals were additionally implanted with an infusion cannula (C315G/SPC, Plastic One) targeting their left VPm. After a post-surgery recovery period, animals were trained to perform a tactile frequency discrimination task while head-fixed. Each trial, a 500 ms sinusoidal waveform whisker deflection of 8, 6, or 4 Hz frequency was delivered to whisker D2 using a piezoelectric bimorph actuator 1 s after an onset tone. An 8 Hz waveform was randomly designated as the go stimulus for all animals. A 4 Hz waveform was designated as no-go stimulus for 2 animals, and a 4 Hz and a 6 Hz waveform were designated as no-go stimuli for the remaining 3 animals. White-noise sound (~90 dB) was continuously played during the task to mask possible auditory cues generated by the piezoelectric actuator. The animals were then required to lick within a 1.2 s window if the go stimulus was presented and withhold a response to any no-go stimuli. If animals correctly responded to a go stimulus, they received an 80 µl water reward aligned with a reward tone. Following a false alarm (FA), the animals entered a 10 s timeout period beginning with a time-out tone. In addition, a 4 s inter-trial interval preceded each new trial irrespective of the previous response. The behavioral apparatus was controlled by an xPC target real-time system (Mathworks) running at 1 kHz and all animal responses were logged for offline analyses. Perceptual sensitivity (d') was calculated from hit rate and FA rate as:

$$d' = \Phi^{-1}(\text{Hit rate}) - \Phi^{-1}(\text{FA rate})$$

where Φ^{-1} is the inverse normal cumulative distribution function. After the animal became proficient in the detection task (hit rate > FA rate for 5 consecutive days), we tested the effects of LC activation on the animal's behavioral performance. Photostimulation of the LC was delivered in blocks of 40 trials alternating with 40 control trials to match the LC activation conditions used in the acute setup. During photostimulation blocks, laser pulses (20 mW mm^{-2}, pulse length 15 ms) were delivered to the LC at 5 Hz throughout the block. Normalized increase in perceptual sensitivity by LC activation was calculated for both 6 Hz and 4 Hz distractors as:

$$\text{Normalized increase in } d' = \frac{d'_{LC\ stim} - d'_{control}}{d'_{LC\ stim} + d'_{control}}$$

On a subset of experiments, the three rats implanted with an infusion cannula were lightly anesthetized with isoflurane before the behavioral task. Approximately 2 µl of sterile phentolamine (10 mM) or saline (as a control) was slowly infused into the thalamus. Following completion of infusion, the animals were allowed to wake up and recover ~45 min before the behavioral task.

Modeling. To facilitate our investigation of how the LC–NE system modulates feature selectivity in the VPm, we created a simplified model of the intrathalamic circuit consisting of a single VPm and a single TRN neuron (Fig. 7a). The TRN neuron received excitatory input from the VPm neuron and in turn provided inhibitory input back to the VPm neuron as well as to itself. An IFB model was used to simulate the TRN and VPm neurons. The input of the VPm model neuron was randomly drawn from a collection of responses of an experimentally recorded PrV neuron to repeated frozen WGN whisker stimulus. For each of the 100 simulated responses of the model neuron, the input was a summation of 5 randomly selected trials from the set of recorded PrV neurons responses. We then performed reverse correlation analysis of the resulting VPm response relative to the WGN whisker stimulus.

The modeled VPm and TRN neurons were constructed using a single compartment that contained 4 membrane currents $I_{membrane}$ and 3 synaptic currents $I_{synaptic}$.

$$\tau\left(\frac{dV}{dt}\right) = R_m\left(\sum I_{membrane} + \sum I_{synaptic}\right)$$

where V was the membrane potential, time constant $\tau = 5$ ms, and membrane resistance $R_m = 20$ MΩ. When the modeled neuron's membrane potential crossed a threshold (spike threshold potential = −40 mV) a spike was generated, and membrane potential was reset (reset potential = −48 mV). Membrane currents were modeled using differential equations and exponential integration methods[32]. The magnitude of each of the membrane currents was calculated at each time step. The current contributed by the potassium leak channel was calculated as: $I_{leak} = G_{leak} \times (E_{leak} - V)$ with $E_{leak} = -85$ mV, where G represents conductance and E represents the reversal potential. G_{leak} was set for each neuron at a level which resulted in firing and bursting rates comparable to those observed in vivo (average G_{leak} of 1.5 ± 0.4 nS for VPm neurons and 4.5 ± 0 nS for TRN neurons). The fast and slow potassium channels currents were calculated as $I_{K_i} = G_K \times D_{K_i} \times (E_K - V)$ with $E_K = -85$ mV. Where G_K limits the max conductance and is equal to 0.5 nS. Whenever the model neuron fired a spike, potassium conductance factor (D_{K_i}) was increased by a fixed amount A_{K_i} and decayed with time constant T_{K_i} using the following equation:

$$\frac{dD_{K_i}}{dt} = \frac{-D_{K_i} + A_{K_i} \times H_K}{T_{K_i}}$$

where H_K equals 1 if a spike has been fired and 0 at all other times. For the fast potassium channels that acted as a delayed rectifier $A_{K_1} = 20$ and $T_{K_1} = 5$ ms. For the slow potassium channels $A_{K_2} = 5$ and $T_{K_2} = 100$ ms (ref. [32]). In addition, the neurons have a voltage-dependent calcium T-channel[55] with current $I_T = G_T \times B_T \times H_T \times (E_T - V)$ with $E_T = 120$ mV and G_T set for each neuron at a level that resulted in a physiologically relevant bursting rate (average G_T of 28 ± 0.5 nS for both TRN and VPm neurons). H_T is set to 1 if the neuron's membrane potential is greater than the hyperpolarization threshold (hyperpolarization threshold = −50 mV) or 0 at all other times. B_T represents the fraction of calcium T-channels that are de-inactivated at any instant and varies between 0 and 1, with value increasing when the neuron's membrane potential is beneath the hyperpolarization threshold as $\frac{dB_T}{dt} = \frac{1 - B_T}{T_{B_{increasing}}}$ and value decreasing when the neuron's membrane potential is above the hyperpolarization threshold as $\frac{dB_T}{dt} = \frac{-B_T}{T_{B_{decreasing}}}$. $T_{B_{increasing}}$ was set to 60 ms which results in ~80% of calcium T-channels being de-inactivated after 100 ms of hyperpolarization and $T_{B_{decreasing}}$ was set to 3 ms which results in inactivation of 99% of calcium T-channels after 10 ms of membrane potential exceeding the hyperpolarization threshold.

Currents due to postsynaptic potentials (PSPs) were calculated as: $I_{PSP} = G_{PSP} \times C_{PSP} \times (E_{PSP} - V)$ where G_{PSP} is the max possible conductance for that PSP type and C_{PSP} represents the strength of conductance relative to the last occurrence of a input spike. For glutamate EPSPs $E_{EPSP} = 0$ mV and G_{EPSP} was set for each neuron at a level that resulted in a physiologically relevant firing rate (average $G_{EPSP} = 120 \pm 28$ nS for VPm neurons and $1{,}010 \pm 85$ nS for TRN neurons). For both $GABA_A$ and $GABA_B$ inhibitory PSPs (IPSPs), $E_{IPSP} = -85$ mV and G_{IPSP} was set for each neuron at a level which resulted in a physiologically relevant firing rate (average $GABA_A$ $G_{IPSP} = 13{,}230 \pm 430$ nS for both VPm neurons and TRN neurons, average $GABA_B$ $G_{IPSP} = 810 \pm 270$ nS for VPm neurons and 550 ± 180 nS for TRN neurons). For all PSPs, the time course of C_{PSP} strength was modeled using dual-alpha function equations with the value of C_{PSP} following a spike calculated as:

$$C_{PSP} = \frac{1}{T_{C_1} - T_{C_2}} \times \left(e^{-\frac{t}{T_{C_1}}} - e^{-\frac{t}{T_{C_2}}} \right)$$

where t is the time after input spike received. For glutamate EPSPs, $T_{C_1} = 0.9$ ms and $T_{C_2} = 2.5$ ms, which results in a EPSP with a max conductance at ~1–2 ms following input which decays in ~15 ms. For $GABA_A$ IPSPs, $T_{C_1} = 2.5$ ms and $T_{C_2} = 15$ ms, which results in an IPSP with a max conductance at ~5 ms following input that decays in ~100 ms. For $GABA_B$ IPSPs, $T_{C_1} = 90$ ms and $T_{C_2} = 100$ ms, which results in an IPSP with a max conductance at ~205 ms following input that decays in ~300 ms. Whenever a PSP was generated due to an incoming spike, a dual-alpha function as described above was added into the vector of C_{PSP}, which allowed for PSPs for to be temporally summed.

These parameters above resulted in a population of VPm neurons on which we can simulate the effects of NE. In this model, to simulate the effects of increased NE concentration, we decreased the strength of the hyperpolarizing leak current to simulate the depolarizing effects of NE (average G_{leak} with NE of 0.5 ± 0.02 nS for both VPm and TRN neurons) and increased the amplitude of post-synaptic potentials to simulate NE-induced increased efficacy of neurotransmitters glutamate (average G_{EPSP} with NE = 370 ± 45 nS for VPm neurons and $1{,}610 \pm 190$ nS for TRN neurons), $GABA_A$ (average $GABA_A$ G_{IPSP} with NE = $15{,}230 \pm 200$ nS for VPm neurons and $15{,}040 \pm 70$ nS for TRN neurons), and $GABA_B$ (average $GABA_B$ G_{IPSP} with NE = $23{,}460 \pm 660$ nS for both VPm and TRN neurons)[32]. Further, we were able to use the model to investigate the effects of NE selectively in the VPm only or the TRN only by selectively changing these parameters for the modeled VPm or TRN neuron only. Finally, we also investigated the effects of removing calcium T-channels in the VPm only, TRN only, or both which allowed us to tease apart their effects on thalamic feature selectivity.

Histology. The animal's brain was fixed in 4% paraformaldehyde in phosphate buffered saline for up to 24 h at 4 °C and cryoprotected in increasing concentrations of sucrose (10%, 20%, 30%) for 24 h each or until the tissue sank to the bottom of the container. Brain tissue was sectioned coronally at 20 µm using a freezing microtome (Leica Microsystems). Slides used for confirming electrode placement were either Nissl stained or stained for cytochrome oxidase. Slides used for confirmation of selective lentiviral expression where immunohistochemically analyzed for the expression of tyrosine hydroxylase (expressed in LC neurons, sheep anti-tyrosine hydroxylase primary antibody, EMD Millipore, Alexa Fluor 488 donkey anti-sheep immunoglobulin-G secondary antibody, Jackson Imunno Research) and mCherry (reporter protein, Mouse Living Colors DsRed polyclonal primary antibody, Clontech, Alexa Fluor 594 donkey anti-mouse immunoglobulin-G, Jackson Imunno Research). Slides were then coverslipped with Permount mounting medium (ThermoFischer Scientific), and were examined using an Olympus CKX41 inverted microscope (Center Valley). Images were stitched together with Microsoft Image Composite Editor.

Statistics. All statistical tests were two-sided. A one-sample Kolmogorov–Smirnov test was used to assess the normality of data before performing statistical tests. If the samples were normally distributed, a paired or unpaired *t*-test was used. Otherwise, the two-sided Mann–Whitney *U*-test was used for unpaired samples or the two-sided Wilcoxon signed-rank test for paired samples. Bonferroni correction was used for multiple comparisons. No statistical methods were used to predetermine sample sizes, but our sample sizes are similar to those in previous reports and are typical for the field. Stimulus randomization was generated by using Matlab random number generators. Data collection and analysis were not performed blind to the conditions of the experiments.

Reporting Summary. Further information on research design is available in the Nature Research Reporting Summary linked to this article.

Code availability. Custom code used in this study is available from the corresponding author upon reasonable request.

Data availability

The data that support the findings of this study are available from the corresponding author upon reasonable request.

References

51. Minnery, B. S. & Simons, D. J. Response properties of whisker-associated trigeminothalamic neurons in rat nucleus principalis. *J. Neurophysiol.* **89**, 40–56 (2003).
52. Xiang, Z. et al. The discovery and characterization of ML218: a novel, centrally active T-Type calcium channel inhibitor with robust effects in STN neurons and in a rodent model of parkinson's disease. *ACS Chem. Neurosci.* **2**, 730–742 (2011).
53. Moore, J. D. et al. Hierarchy of orofacial rhythms revealed through whisking and breathing. *Nature* **497**, 205–210 (2013).
54. Schwartz, O., Pillow, J. W., Rust, N. C. & Simoncelli, E. P. Spike-triggered neural characterization. *J. Vis.* **6**, 484–507 (2006).
55. Lesica, N. A. et al. Dynamic encoding of natural luminance sequences by LGN bursts. *PLoS Biol.* **4**, e209 (2006).